TECHNISCHE UNIVERSITÄT WIEN
Vienna | Austria

Master Thesis

Applications of ToF-SIMS in modern Material Science

Carried out for the purpose of obtaining the degree of Master of Science

submitted at TU Wien, Faculty of Technical Chemistry

by

Jakob Rath BSc.

Mat.Nr.: 01308809

Oisberg 3, 3343, Hollenstein an der Ybbs

Under the supervision of

Ao. Prof. Dr.$_{tech}$ Dipl.Ing, Herbert Hutter

Research Group for Chemical Technologies and Analytics

Vienna, September 2019

Acknowledgements:

First of all I would like to thank Professor Herbert “Hörby” Hutter for the chance to work under his supervision performing measurements on a device, that is not only one of the most expensive but also the most interesting machine I have ever worked with. Even though I had some tough days during these six months, he always believed in me, which helped me a lot. Always stay as you are Hörby.

I would also like to thank all the members in the working group, who were always there with advice whenever I needed something. Especially Anna Bleier and Lukas Volgger became esteemed friends and supported me in scientific as well as personal matters.

Of course, I want to thank my family and friends, who always tended to believe more in my capability then I did. I would not be the same person without your great support during these last years.

Due to reasons of space, I am not going to mention all the people, who are important in my life by name but I think, and hope, that those, who helped me most probably know what they mean to me.

Abstract:

ToF-SIMS is one of the most sophisticated state-of-the-art techniques applicable in a broad field of material science. It allows the detection of all elements from hydrogen to uranium usually in a concentration region of ppm to ppb with high mass as well as spatial resolution. In addition, depth profiles with a depth resolution of about two atomic monolayers enable the operator to investigate surface and interface phenomena and perform measurements for determination of diffusion properties with a precision, that cannot be reached with any other method.

In this thesis, samples of diverse types and compositions were investigated under various operation conditions resulting in a range of material properties being obtained. Whilst high spatial resolution measurements on steel samples were performed in order to understand the mechanisms behind the distribution and segregation of single alloy components during manufacturing and processing, diffusive properties of various insulating and semiconducting samples were determined by performing measurements with higher ion currents and increased mass resolution instead.

The obtained data shows that ToF-SIMS measurements offer an enormous and unique potential for definition and understanding of various material properties and play an essential role in technological development.

Deutsche Kurzfassung:

ToF-SIMS ist eine der höchstentwickelten “state-of-the-art” Techniken, die in einem weiten Bereich materialwissenschaftlicher Forschung angewandt werden kann. Die Methode erlaubt die Detektion aller Elemente von Wasserstoff bis Uran bis hin zu Konzentrationen von wenigen ppm oder ppb mit hoher räumlicher- sowie Massenauflösung. Zusätzlich erlaubt das Aufnehmen von Tiefenprofilen, die mit einer Tiefenschärfe von ein bis zwei atomaren Monolagen aufgezeichnet werden, eine Untersuchung von Ober- und Grenzflächen-Phänomenen sowie die Bestimmung von Diffusionskoeffizienten mit einer Präzision, die von keiner anderen Technik erreicht wird.

In dieser Arbeit wurden verschiedenste Proben unter unterschiedlichen Betriebsbedingungen untersucht, wobei eine Bandbreite an Materialeigenschaften bestimmt werden konnte. Während die räumliche Verteilung verschiedenster Legierungskomponenten einiger Stahlproben mithilfe hoch-ortsauflösender Messungen bestimmt wurde, konnten die Diffusionseigenschaften unterschiedlicher Teilchen in nichtmetallischer Matrix durch Messungen unter höheren Ionenströmen und höherer Massenauflösung bestimmt werden.

Die erhaltenen Messwerte zeigen, dass die Methode ToF-SIMS ein enormes sowie einzigartiges Potential bietet um zum Verständnis und zur Beschreibung unterschiedlichster Materialeigenschaften beitragen und eine wichtige Rolle in der Entwicklung neuer Werkstoffe spielen kann.

Motivation:

Within this thesis, various applications for time of flight secondary ion mass spectrometry (ToF-SIMS) have been developed and improved in order to advance and optimise manufacturing, processing or general understanding of different materials. To cover a broad variety of different scientific interests, several cooperation projects were organized with both, working groups from universities as well as large European material manufacturers. By performing measurements on a range of samples with completely different requirements, one is able to develop advanced general understanding on the principles of ToF-SIMS and optimise settings for any demand.

Some studies focussed on the determination of diffusion kinetics, where the device was usually operated under conditions of high mass resolution. In other applications, the spatial resolution was maximised in order to perform imaging in the sub-micron range for determination of elemental distribution across microstructures of different alloys.

Table of Content:

1) Introduction

1.1) ToF-SIMS

1.1.1) Concept

Time of Flight Secondary Ion Mass Spectrometry (ToF-SIMS) is the dominant variant of static SIMS and a highly sensitive method for trace analysis (up to ppm/ppb) of surfaces, thin films as well as interfaces. The technique provides information about surface physics and chemistry on a very detailed level. By use of ToF-SIMS it is possible to obtain molecular and elemental information of inorganic and organic systems on a three-dimensional scale with high mass and spatial resolution.

SIMS is a highly specialised form of mass spectrometry of ionised particles which are emitted by bombarding a surface with a focussed beam of heavy "primary" ions. This process leads to emission of electrons, neutrals as well as atomic and cluster ions from the surface of the specimen. The energy of the primary ions is transferred to particles from the uppermost sample monolayers by a collision-cascade. Only a small part of these collisions is transferred back to atoms and molecules in the top layer of which a low number develops enough energy to overcome surface binding and is accelerated towards a mass analyser. This process of emission of secondary particles is called sputtering. As primary ions, mainly Ar^+, Ga^+, Cs^+ or – as in the case of our studies – Bi^+ are utilized. For special applications and high mass samples the use of cluster primary ions as SF_5^+, Au_n^+ or Ar_{1000}^+ offers some great advantages. The major part of sputtered particles consists of neutrals in form of atoms or molecules and is lost for analytical purpose of SIMS. Only charged secondary particles are detected and analysed by a ToF mass spectrometer. As this method is basically destructive as primary and sputtered ions might affect the chemistry of the surface it is necessary to keep the dose of primary ions very low to make this effect negligible. The generated secondary ions are collected by an extractor and following analysed in a reflectron time of flight (ToF) mass spectrometer (MS) providing detailed information

on composition of the observed surface. The functionality of this ToF-MS is based on an electrical field which accelerates the ions and a subsequent drift region leading to a detector – usually a micro-channel plate (MCP). Separation of ions is achieved via mass per charge unit (m/z). Lighter ions travel with higher velocity and therefore appear at the detector unit earlier. The reflectron (ion mirror) has the role to compensate small differences in initial energy and sputtering angle of the secondary ions to increase mass resolution. Due to the input of positive charge in the form of primary cations during the process of sputtering, the surface of insulating samples is getting charged. The positive surface potential increases rapidly such that the kinetic energy of the positive secondary ions rises well behind the acceptance window of the analyser. The problem of surface charging is compensated by irradiating the sample with a flood gun, emitting a beam of relatively low energy electrons.[1] By decreasing the spot size of the LMIG and rastering the pulsed primary beam over the sample surface it is possible to determine the lateral distribution of elements and molecules with very high resolution for imaging. A schematic view of the applied ToF.SIMS 5 device is shown in figure 1, explanations of the single compounds are provided in section 1.1.2).

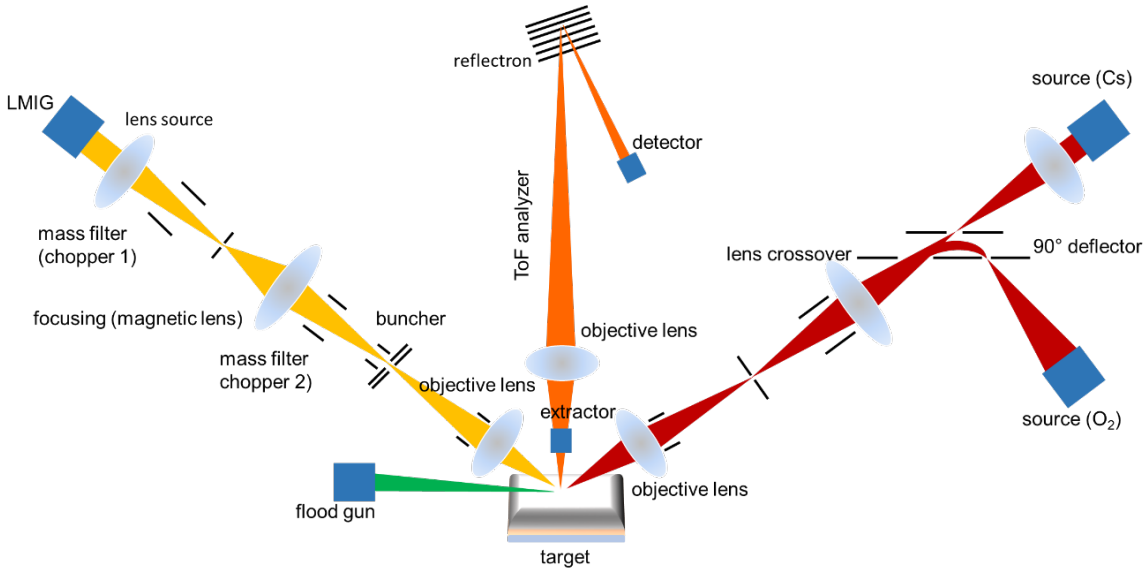

Figure 1: Schematic illustration of the TOF.SIMS 5 device utilized for the measurements performed in this thesis: The left part of the picture presents the ion optical column of the analysis beam (yellow), the red beam and associated components sketched in the right correspond to the dual source column of the etching beam. The beam of secondary ions is illustrated in orange. Kindly provided by Anna Bleier, TU Vienna.

1.1.2) Detailed View

1.1.2.1) Generation of Primary Beam

In ToF-SIMS devices, a beam of high energy ions is pulsed by use of mass filters (choppers) and rastered over the surface of a sample by use of advanced ion optical columns. Subsequently pulses of secondary ions emitting from the upper monolayers are produced. In modern units, there is more than one primary beam in use. The „analysis beam“ produces secondary ions for analytical purpose whilst the „etching beam“ or „sputter gun“ removes material from the top layers to obtain a stepwise depth profiling of the observed sample. Generally, there are three different types of ion sources utilized in SIMS measurements: liquid metal ion sources/guns (LMIS/LMIG), surface ionisation sources and gas sources. The IONTOF ToF.SIMS 5 contains one of each source for different requirements.

LMIS are most broadly used in ToF-SIMS devices, common employed metals are Gallium and Bismuth. The analysis gun in the IONTOF ToF.SIMS 5 is equipped with a BiMn reservoir that provides a more stable emission current compared to pure Bi. These pieces of equipment consist of a metal reservoir linked with a Wolfram needle that is welded to a heater filament that in turn is connected to two support legs serving as electrical contacts. These legs are again placed in an insulating disc and are supplied to a high positive voltage. An illustration of an LMIG is provided in figure 2. The temperature of the needle is set to a value at which the bismuth remains liquid and coats the tip with a thin film of molten metal. Close to the tip of the needle, a circular extraction electrode with applied voltages between -5 and -10 kV relative to the source is arranged. Metal ions surrounding the source are responding to the strong electric field by migrating towards the anode whilst electrons move in the opposite direction towards the high positive voltage. This behaviour leads to the formation of a cone at the tip of the needle, the so-called Taylor cone, which reaches equilibrium state between surface tension and electrostatic forces when its half

angles obtain a value of 49.3 °. This is when emission of ions starts on top of the spike. This state is followed by a state of dynamic equilibrium with a constant flux of ions leaving the tip. The emission area of liquid metal ion guns can be as small as 10 nm (in case of Ga) and therefore is capable of releasing a bright and narrow beam of Cations onto the sample surface. Depending on demanded surface tension, mass, flowing and melting properties, there are four different metals used in LMIS construction. Whilst Ga is used due to its very low melting point and beneficial flow characteristics, Bi is used because of its higher atomic masses – resulting in higher sputter rates - and relatively low melting points. Additionally, Bi only forms one "stable" isotope and facilitates extended analytical possibilities due to its ambition to give rise to cluster ions. Au is used because of its high atomic mass and tendency to form cluster ions. The disadvantage of gold is its high melting point and the propensity to vaporise under conditions of evanescent pressure. [2]

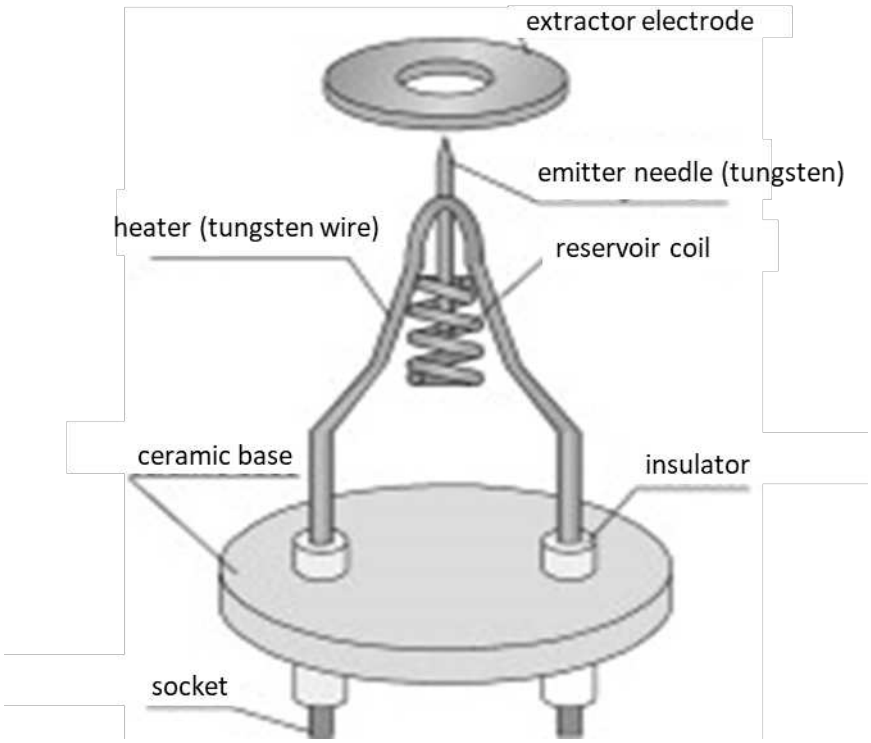

Figure 2: Illustration of a liquid metal ion gun: The tungsten emitter is welded to reservoir coil as well as a tungsten heating wire, thermal insulation is provided by ceramic disc, the beam of ions is extracted from the tip of the tungsten needle by a circular extractor electrode. Source: Jaworek, A., 2007, S. 18 [3]

For detection of secondary ions with negative charge (e.g. oxygen), surface ionisation sources – mainly condensing Cs particles on the tip of a heated tungsten filament - are employed as etching beams. Formation of caesium ions is a function of the elemental ionisation energy as well as temperature of the filament and the work function of W. By migration of electrons to the cathode the Cations are released, extracted to an electron optical column and focused to the measuring spot. Relatively to LMIS guns, ion beams emitted from a Cs filament show higher currents and lower energy spreads but have poorer luminous intensities. [4]

In gas or plasma ion sources positive as well as negative charged ions can be formed. In this type of ion source, a gas – usually a noble gas or oxygen – is injected into the space inside a grid, that is surrounded by a circular filament cathode which is inducing electrons and forcing them to rotate on circular paths in this region of the grid. By bombarding gas atoms/molecules with electrons, ionisation occurs. The so formed charged particles are extracted by an electric field right after generation and then focused in an electron optical column. A modern and powerful variety of plasma ion sources is the duoplasmatron which uses light arcs between electrodes in the gas stream for formation of ions. Usually ion beams produced in gas sources have a higher brightness and weaker spatial resolution than beams produced in LMIS and surface ionisation sources. Gas sources are applied as both - etching beams as well as analysis beams. [5]

In the ToF-SIMS 5 device utilized for the experiments painted in this thesis all three types of primary guns explained above were applied. The analysis beam is a BiMn-LMIG, for etching a dual source column (DSC) containing a Cs (surface ionisation) emitter as well as an oxygen gas source is included. By alternate emission of ion beams from the LMIG and one of the two guns of the DSC depth profiles as well as 3D images of the observed sample can be generated.

1.1.2.2) Generation of Secondary Ions

The formation of secondary ions in ToF-SIMS experiments occurs because of interactions of heavy, highly energetic primary ions with particles in the sample surface due to so-called collision cascades. In the utilized ToF.SIMS 5 device a 25 kV beam of bismuth ions penetrates the sample surface transferring their energy and momentum to atoms and molecules in the surface monolayer. These are subsequently passing the energy to bulk atoms in a billiard ball type behaviour and so on. However, there is a chance that some of these collisions proceed in a manner that energy is passed over several stations until another particle on the surface is hit. If the kinetic energy passed with this strike is higher than the binding energy of this specific particle it is knocked out of the sample and can be detected in the integrated reflector time-of-flight mass spectrometer. However, most of the particles knocked out during the sputtering process are electrons and neutrals whereas ionized species represent only 5 per cent of the total amount of events. Figure 3 illustrates the process of sputtering.

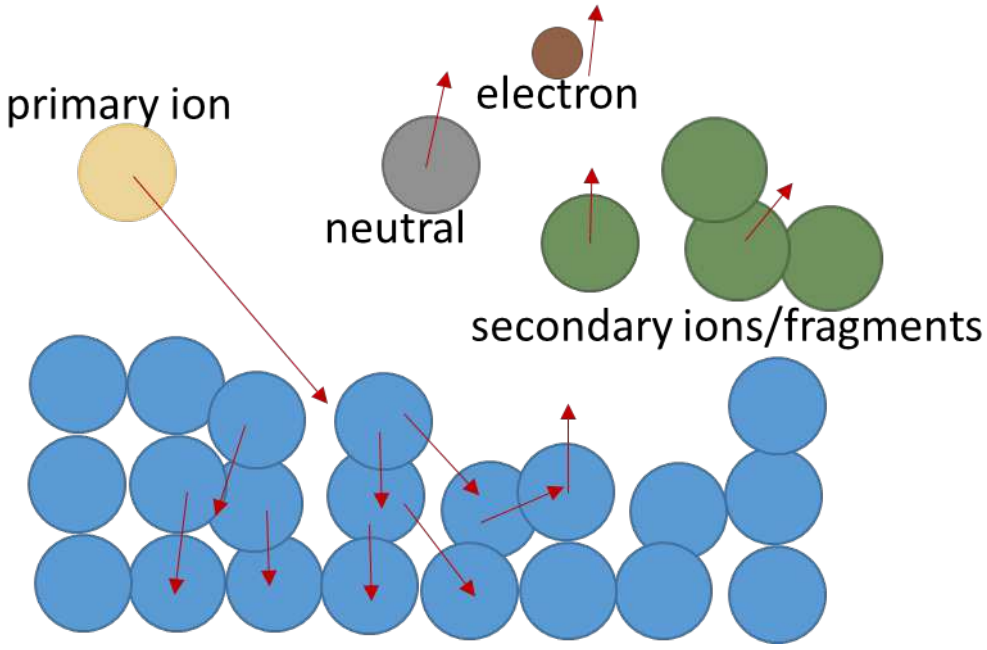

Figure 3: The mechanism of sputtering: A beam of heavy primary ions (yellow) penetrates the surface of a sample triggering billiard ball like collision cascades leading to the emission of neutrals (grey) electrons (brown) and charged secondary particles (green). While 95 % of all emitted particles are either neutrals or electrons, secondary ions and fragments that are subsequently used for analytical purposes only account for 5 %.

The amount of secondary ions that is formed by irradiating a sample's surface with an ion beam is described by the following simplified equation, which can be seen as the basic SIMS equation.

$$I_m = I_{in} * Y_m * \alpha^{+/-} * \theta_m * \eta \qquad (1)$$

I_m is the intensity of the flux of a specific secondary particle m, I_{in} is the initial intensity of the primary ion beam, Y_m is the so-called sputter yield of the implied particle, $\alpha^{+/-}$ is its probability of ionisation to form positive or negative ions, θ_m is the fractional concentration of species m and η is the transmission of the analysis system. [6,7]

For analytical purposes, Y_m and α^+ are the two most eminent parameters. The sputter yield of a specific element is a sum signal for all neutral and charged species emitted from the surface after bombardment with a primary beam. It is directly proportional to the primary flux and increases with charge, energy and mass of the primary particle. Also, the microstructure of the specimen and form and composition of the matrix strongly affects the yield of secondary particles necessitating sound considerations when evaluating data of samples with changing matrix phases for instance thin layer systems. For a given primary beam energy the sputter yield varies by a factor of three to five through the whole periodic table.

The ionisation probability of a certain species strongly depends on electron exchange processes occurring between the surface of the sample and the escaping elemental or molecular particles. The yield for secondary ions can vary by six orders of magnitude through the periodic table and is additionally affected by the electronic and chemical state of the surrounding phase. This matrix effect leads to very different results when investigating one and the same element in a metallic or ceramic material. [8]

When performing SIMS experiments on semiconducting or insulating samples, the bombardment of the surface with a primary beam of positive ions leads to positive surface charging. Due to the input of positive charge and subsequent emission of secondary electrons the surface potential may rise to a value of several hundred volts

decreasing the velocity of the secondary ions beyond the acceptance window of the analyser unit. [9] In addition the positive surface potential may promote the migration of electro-positive species (e.g. alkali metals) towards the bulk. To solve these problems and to compensate for the positive surface potential the specimen can be put in electrical contact with the stage for example by use of conductive tape or by depositing a thin film of the sample on silver foil. Alternatively, the surface of the specimen can be irradiated with a beam of low energy electrons from a so-called flood gun. The energy of these electrons is about 21 eV enabling a self-adjusting charge compensation without sample damaging due to emission of secondary particles. [10]

1.1.2.3) Analyser Unit

The first application of a time of flight mass analyser in a SIMS experiment was introduced by Chait and Standing in 1981. They utilized a 10 kV Cs^+ primary source followed by a 2 m long linear ToF spectrometer connected to a double micro channel plate. By doing so, they could reach mass resolutions of $m/\Delta m \approx 3.000$. In modern ToF-SIMS devices the linear time of flight analyser is replaced by a reflectron ToF allowing the operator energy compensation of the secondary ions increasing the mass resolution to a value of up to 11.000. [11]

When a pulse of primary ions in the range of ns impacts onto the surface of the sample, emission of a beam of secondary ions is the immediate consequence. The period between two single pulses determines the measuring time of the ToF analyser. The charged particles that are formed at the sample surface are accelerated by an electrostatic extraction unit and transmitted into the drift region of the mass spectrometer. There all ions of the same polarity (in order positive or negative charged) are accelerated up to the same nominal kinetic energy before they enter the field-free drift region where they are separated due to different molecular masses. The time until a particular ion is detected is directly proportional to the

length of the drift region as well as the square root of the ions molecular mass which means that ions with smaller masses are detected earlier and separation between the single peaks is better for light ions than for heavier ones. Therefore, the duration of the experimental process depends on the observed mass range of the analyte. One of the greatest advantages of time of flight mass spectrometers is the possibility – depending on the detector efficiency - to detect all ion masses that are emitted from the surface of the specimen simultaneously. On the other hand, mass spectrometers working with magnetic sectors are limited to only one specific mass to charge ratio at one time explaining the high overall detection sensitivity of ToF-SIMS. As masses of unlimited range are detectable in the ToF analyser the rate of pulsing and subsequent measurements is limited. If only lower masse are interesting to the operator but the sample surface emits ions with very high weight as well, some of these impacts might not be detected in the current detection period but already in the following sequence causing the appearance of unjustified peaks at irregular masses. To avoid this situation, it is possible to either apply a blanking system limiting the mass range of the secondary ion pulse or to set the pulse period duration to a value low enough.

The mass resolution that can be reached by the ToF analyser directly correlates to the length of the primary ion pulse, the mass range of interest and the length of the drift region. In any linear ToF spectrometer the strongest limitation for the maximum achievable mass resolution would be the distribution in kinetic energy of the secondary particles that is caused by the unspecific energy loss during any single step of the collision cascade. As a consequence, ions of the same mass are dispersing in the drift region whereat an increase of flight time will not improve the accessible mass resolution. By introducing an reflectron it is possible to compensate for the energy spread of the secondary ions. The reflectron ToF analyser is a combination of at least two drift regions with a reflectron in between. By utilization of several electrostatic fields with increasing applied voltages the beam of secondary ions is reflected on a second field free area leading to an increased drift region within the same geometrical size of the measuring device as well as an improved mass resolution. When arriving in the field free region of the ToF analyser two ions of the

same nominal mass are moving towards the electrostatic reflectron. As their initial kinetic energies are not exactly the same due to different collision pathways during the ions creation an ion with higher kinetic energy has a higher velocity leading to an increasing distance between particles of same mass during flight time. When entering the field of the reflectron the ions are decelerated, stopped and subsequently accelerated onto another drift region connected to a detector. Ions of higher kinetic energy are penetrating the mirror deeper where they are influenced by stronger fields. When inversion of the direction occurs the low energy ions are ahead the higher energy ones. As the forces applied in greater depth of the mirror are stronger, the ions with higher initial energies are accelerated to a higher speed. In case of an ideally aligned mirror voltage, they catch up with the ions of same mass but lower speed at the surface of the detector unit simultaneously leading to a maximum mass resolution of $m/\Delta m > 10.000$. An illustration of a reflectron ToF mass analyser is provided in figure 5. [12]

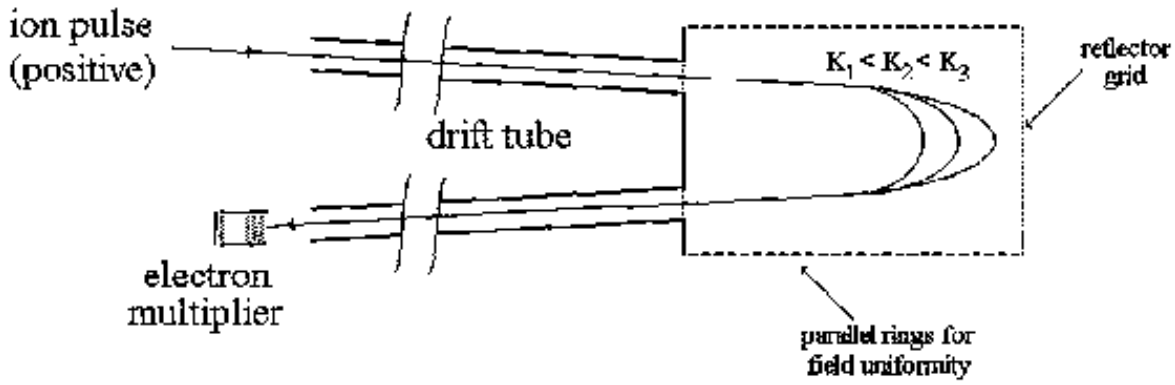

Figure 4: Schematic of a reflectron ToF mass analyzer utilized in an ToF-SIMS device: The pulse of secondary ions is emitted from the surface of the sample and moves along the first drift region where ions of same mass are separated as their initial energies are distributed,. Subsequently the ions are decelerated in the region of the electrostatic field of the reflectron where ions with higher velocity (K) penetrate the mirror deeper than slower particles. With increasing penetration depth, the voltages applied to the electrostatic fields of the reflectron increase. All ions are reflected onto a second drift region and following detected by use of a microi channel plate detector. With an ideally aligned reflector system all particles of same mass arrive at the detection unit simultaneously. Source: Amoruso, S., et al., 1999 [13]

1.1.2.4) Measuring Modes

Depending on the analytical requirements and the type of sample observed there are different demands for the analysis beam. For analysis of semi-conducting samples, one might be interested in high spatial resolution images whilst someone working on organic materials would rather like to maximise mass resolution. Of course, all these specifications are interdependent which sometimes necessitates taking compromises for gaining performance. For static analysis conditions, it is important that the observed sample area was not damaged by previous ion bombardment which implies that no point of the surface should be hit by more than one ion. The limit for these requirements is accepted to be 10^{13} impacts per square centimetre and is called the static limit. It is directly proportional to the irradiated sample area and indirectly proportional to the intensity of the primary beam as well as the sputter yield Y_m of the investigated species m. [14] Usually measurements are performed close to this value to obtain maximum surface data without registration of damaged regions. Setting the primary beam to a value underneath the static limit can either be achieved by decreasing the primary ion current or – more likely – by decreasing the pulse length.

The main influences of the spatial resolution in ToF-SIMS devices are the lenses, the apertures, the pulsing unit and the electrical supply for the ion-optical column. For maximising spatial resolution only ions from a certain point of the tip, with limited angular acceptance and energy spread can be used. An ideal aligned ion-optical column meets these requirements by focusing the beam with minimum aberrations, removing unwanted parts of the beam for optimization of the spot diameter, eliminating neutrals and chopping and mass filtering it in order to increase mass resolution. Even though it is possible to focus a beam by use of only one lens, introduction of a second lens enables generation of beams with different magnification. In general, a beam produced in any type of ion source enters the first ion-optical lens that either can focus the beam in a certain spot or can collimate it. These ions are subsequently sent through the remaining parts of the ion-optical

system to a second lens that focuses the beam onto the sample surface. Modern devices usually operate with three lenses. [15]

In an IONTOF TOF.SIMS 5 instrument, the three magnetic lenses of the 25 kV Bi^+ ion column offer the operator the possibility to adjust the beam guidance in order to optimize the beams properties for any type of scientific requirement. In general, there are three modes suggested by the manufacturer of the utilized device: High current bunched (HCBU), burst alignment (BA) and collimated mode.

While HCBU provides measurements with high mass resolution and beam currents, the BA mode is a multifunctional mode with lower currents and mass resolution but increased lateral resolution up to ~200 nm. The collimated mode with its very low currents and mass resolution is utilized in imaging applications and is the only operating mode abdicating a crossover of the analysis beam. As this mode was not applied in any experimental procedure executed in this thesis, a more detailed illustration is relinquished. Additionally to the measuring modes listed by the manufacturer the collimated burst alignment (CBA) mode, that was developed on the ToF.SIMS 5 device used in this work can be employed for special requirements. [16] The options for beam guidance of the feasible measuring modes are illustrated in figure 6, values for standard operation conditions of the presented modes are given in table 1.

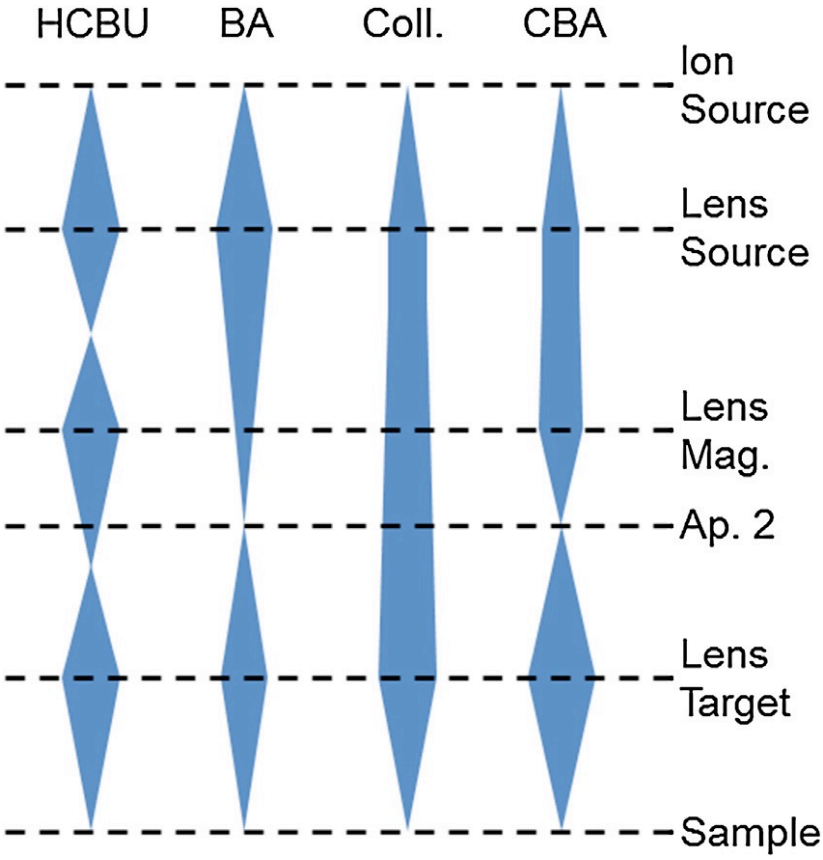

Figure 5: Illustration of the possible beam guidances utilized in ToF-SIMS measurements: The HCBU mode provides high intensities and advanced mass resolution of m/Δm > 10.000 whereas the remaining modes are operating with much lower currents of primary ions and are commonly applied for imaging applications with maximum spatial resolutions of sub 100 nm. Source: Kubicek, M., et al., 2014 [17]

HCBU (High Current Bunched) Mode

As a pulse of primary ions impacting on the surface of the sample has a specific duration, the secondary ions are not formed at the exact same point of time and a reduction of mass resolution occurs. There are different options to maximise mass resolution. One possibility is to use very short pulses (e.g. in the order of few nanoseconds) which unfortunately leads to reduced spatial resolution due to shifts of the beam during the pulsing process.

An alternative is the use of a so-called “buncher”. The principle of this device is to shorten the total length of an ion pulse by compressing it in space. The buncher consists of two plates with concentric central apertures in beam direction. When the pulse of ions is located in between these plates a certain voltage is applied to the rear plate accelerating the back ions towards the sample. If the buncher is well adjusted, the rear ions catch up with the front ones right at the sample surface maximising mass resolution up to $m/\Delta m > 10.000$ by compressing a 20 ns pulse to less than 1 ns at the sample surface. As the rear ions are accelerated it is unavoidable that the charged particles show an energy distribution (chromatic aberration) which in turn decreases spatial resolution to a few µm. [18]

For primary ion sources producing more than one type of charged species mass filters are applied. These so-called pre-choppers are electromagnetic filters placed orthogonal to the beam axis and are able to send ions with favoured velocities (~ m) threw on stable orbits while ions with higher or lower masses are separated and deflected from the optical axis. [19]

For special applications, where high spatial as well as mass resolution is required, some ToF-SIMS devices offer the possibility for post-ionisation of neutral particles formed during the sputtering process. Therefore, neutral particles are illuminated with short laser pulses right above the sample surface greatly enhancing the secondary ion yield. This technique called ToF-SNMS (Secondary Neutral Mass Spectrometry) offers special advantages when observing biological samples but is rarely utilized nowadays. [20]

Inside the path of the ion beam in HCBU mode there are two crossovers producing a spot of about 2-10 µm diameter on the sample. The beam current is considerable higher than in any other measurement mode. Mass resolution reaches its maximum of about $m/\Delta m = 11.000$ whilst spatial resolution is poor due to the large diameter of the focus spot.

BA (Burst Alignment) Mode

Elemental mapping or ion imaging has always been a popular application of ToF-SIMS as graphical representation simplifies understanding of a result. Whereas imaging was mainly executed in the semiconductor industry in the past, other fields as visualisation of diffusion pathways in metallurgy and investigations on biological samples were on the rise within the last decades. When operating a ToF-SIMS in HCBU mode, the beam is guided into two crossovers: One at aperture one and the second underneath aperture two. In BA mode the first focal point is moved down the ion optical column by shifting the voltage applied on lens source and turning off the magnification lens. Subsequently the second crossover vanishes. By setting the crossover down, most of the beam is blanked out in aperture 1 that is 50 µm in diameter leading to a reduced beam intensity as well as a reduced beam diameter of 200-300 nm resulting in an increased spatial resolution. Comparing to a current of about 14 - 17 nA in HCBU (DC mode) the value measured on the target amperometer in BA is about 0.4 - 0.7 nA corresponding to an intensity decrease of a factor of approximately 40. To compensate for the reduced intensity, the pulse duration of the LMIG can be tuned to about 100 ns compared to 20 ns in HCBU mode. As the buncher is turned off in this measuring mode, all primary ions reach the sample surface with the same energy reducing chromatic aberrations. Due to the long pulse duration, mass resolution is decreased to unity. [21] Similarly to electron microscopes the maximum resolution achievable strongly depends on the successful clearance from axial astigmatism originating from the beam forming lenses. Introduction of two stigmator units enables the operator to optimize the properties of the properties of the LMIG beam spot for high spatial resolution measurements. In general, these elements are tuneable cylindrical magnetic lenses. [22]

For achieving measurements with high spatial resolution in the sub 300 nm range as well as sufficient mass resolution of $m/\Delta m > 6.000$ IONTOF introduced the so-called “burst mode”, which is utilized for detection of trace metals and sample mapping. Under standard measuring conditions, secondary ions produced from only one specific pulse of primary ions are passing the ToF to avoid overlap of spectra

generated from different primary bombardments. If the device is operating under the condition of high mass resolution, spectral lines of lower masses are generally widely spaced which allows acquisition and overlap of spectra from up to ten pulses without interference of peaks. By doing so, the amount of secondary ion counts can be increased drastically, which significantly increases the sensitivity and speed of the method. [23]

CBA (Collimated Burst Alignment) Mode

In 2014 a novel operating mode for Tof-SIMS was developed at the institute for chemical technologies and analytics at the Technische Universität (TU) Wien. Comparing to the BA mode lateral resolution is improved while mass resolution is idem when operating both measuring modes in burst mode. The beam guidance of the collimated burst alignment (CBA) mode shows characteristics from both BA and collimated mode explaining the name of the novel technique. By tuning the voltage applied on lens source the beam is kept very parallel as in collimated mode whereas an applied voltage to the magnification lens in the lower part of the ion optical column guides the beam into a crossover at aperture 2, similarly to the guidance in BA. Comparing to BA a slight decrease of the focus depth in CBA mode is explained by the larger beam angle on aperture 2. This necessitates an exact adjustment of the samples height, which is necessary in all SIMS experiments, anyway. Due to the fact, that the setting of the applied voltages on both, Lens Magnification and Lens Source, can be executed with high precision, it is possible to adjust between BA and CBA almost continuously. Setting the voltages on these lenses to values in between those given for BA and CBA offers the possibility to optimize the analysis beam for any specific requirement.

By operating BA and CBA in the so-called burst mode, an increase of mass resolution by a factor of more than 30 ($m/\Delta m$ >6000) can be accomplished. These conditions can be obtained by chopping the primary ion beam to pulses of lengths in the lower

ns region and overlap of spectra from up to ten consecutive pulses. Countermove the intensity is reduced by a factor of 30 as well.

Operation mode	HCBU	BA	Collimated	CBA
Lens Source (Extractor 9 kV)	~3150 V	~3300 V	~3900 V	~3750 V
Lens Magnification	~14.8 kV	0 V	0 V	12-13 kV
DC-current	14-17 nA	0.4-0.7 nA	50 pA	70-100 pA
No. of crossovers	2	1	0	1
Lateral resolution	2-10 µm	~250 nm	~100 nm	~100 nm
Mass resolution	~11000	Unit (~200)	Unit (~200)	Unit (~200)
Burst	x	>6000	impracticable	>6000

Table 1: Standard operation conditions and accessible resolution parameters for the measuring modes obtainable with modern ToF-SIMS devices. Source: Kubicek M., 2014. [24]

1.1.2.5) Depth Profiling: Interlaced/Non-interlaced Mode

The duration of a pulse from the LMIG is 20 ns while a measuring cycle for a mass interval of m/z = 1 to 371 takes 65 µs. Therefore, 99.98 % of the cycle time can be used for removal of material by use of the sputter gun and successive charge compensation. If any LMIG pulse is immediately followed by irradiation of the sample with the etching beam and electron flooding one speaks of interlaced mode.

Whenever required by experimental setup or nature of the investigated sample, complete separation from analysis and sputtering cycle might become essential. The non-interlaced mode consists of a measuring period where a series of analysis frames is followed by a pause time that in turn is followed by a period for etching and charge compensation. A schematic explanation of the two different measurement techniques is provided in figure 6.

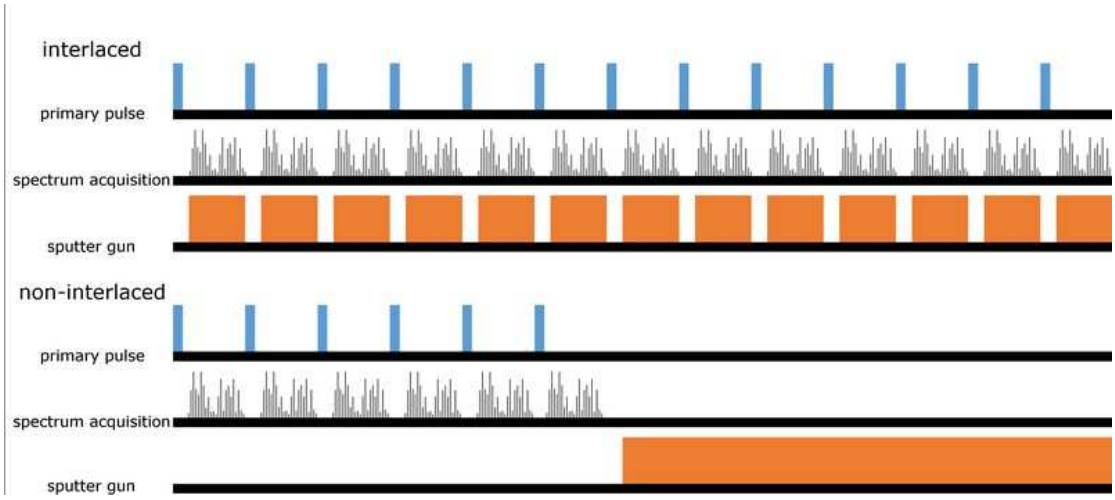

Figure 6: Illustration of the interlaced and non-interlaced measuring mode in ToF-SIMS: Analysis and sputter cycle are completely separated in non-interlaced mode; by doing so the influence of surface charging can be reduced significantly. Kindly provided by Andreas Amsüss, TU Vienna.

While the interlaced mode offers advanced measuring times, the non-interlaced mode provides the option for increased depth resolution, an improved signal-to-noise ratio and reduced surface charging. That is why the non-interlaced mode is broadly utilized in experiments on non-conductive materials.

1.1) Diffusion

Diffusion is the process of transportation of matter from one section of a system to another because of random molecular motion. The movement of each single diffusing molecule can be described in terms of a random walk process. Even though it is possible to calculate the mean square distance travelled within a certain time it is not possible to determine in what direction a specific molecule will move during that period. [25]

1.2.1) Diffusion Equations

When Adolf Fick started working on a mathematical explanation for this complex behaviour, he recognised an analogy between diffusion and heat transfer by conduction which was explained mathematically by Fourier some years earlier. He noticed that the diffusion rate F of a substance through unit area directly correlates to the diffusing substances concentration gradient $\frac{\partial C}{\partial x}$ normal to that area by what we call Fick's first law.

$$F = -D * \left(\frac{\partial C}{\partial x}\right) \qquad (2)$$

Where D is the diffusion coefficient in unit m^2/s of the diffusing substance in an isotropic medium and the negative sign refers to the observation that diffusion always takes place in direction of decreasing concentration. The time dependence of the concentration of a diffusing substance $\frac{\partial C}{\partial t}$ through an area intersection is described by Fick's second law:

$$\frac{\partial C}{\partial t} = -D * \left(\frac{\partial^2 C}{\partial x^2}\right) \qquad (3)$$

This formula was derived by Einstein when reflecting thermodynamic connections between Fick's work and the description of molecular transport by Brownian motion in 1905. [26] The diffusion coefficient is temperature dependent showing an Arrhenius-type behaviour.

$$D = D_0 * e^{-\frac{E_A}{R \times T}} \qquad (4)$$

With D_0 being a function of the interatomic distance, number of vacancies in the matrix material and jump frequency of the diffusing element. E_A is the activation energy for diffusion in a specific matrix, R the universal gas constant (R = 8.314 J/K*mol) and T is the absolute temperature in K. For determination of kinetics of a specific reaction, equation (3) is converted to its logarithmic form (4). Plotting of ln(D) against 1/T results in the Arrhenius plot, a linear function with a slope that correlates to the activation energy of the observed reaction and an intercept with the y-axis that correlates to the maximum diffusion coefficient D_0.

$$\ln(D) = \ln(D_0) - \frac{E_A}{R} \cdot \frac{1}{T} \qquad (5)$$

1.2.2) Harrison's Diffusion Regimes

When describing diffusion on atomic scales differentiation of diffusion into grain boundary and bulk diffusion is essential. L. G. Harrison predicted three interdependent diffusion regimes he called A, B and C to occur in solid, polycrystalline materials. He also provided the possibility to infer from set up time and diffusion length to the type of regime taking place. [27] An illustration of the three different diffusion regimes is given in figure 7.

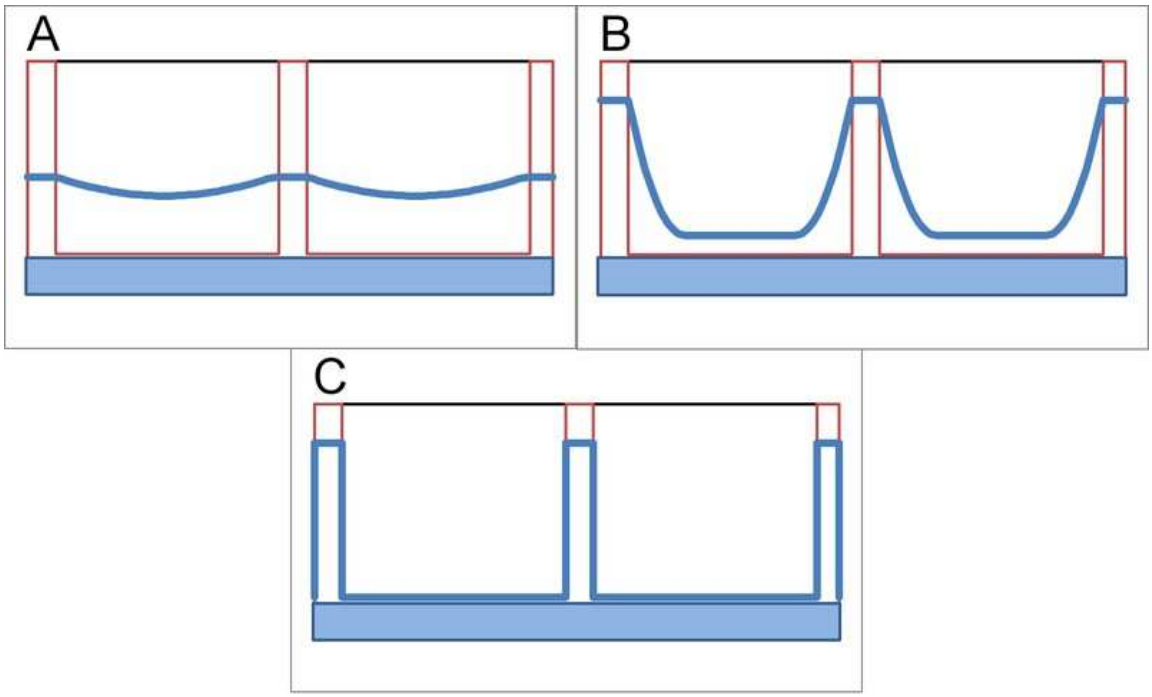

Figure 7: The three mechanisms of diffusion according to Harrison; Regime A: complete bulk diffusion; Regime B: transition state between bulk and grain boundary diffusion; Regime C: complete grain boundary diffusion. Kindly provided by Andreas Amsüss, TU Vienna.

Regime A diffusion occurs for high temperatures, long diffusion times as well as in materials with similar diffusion coefficients for grains and grain boundaries and can be seen as complete bulk diffusion. The diffusion front is approximately plane and

diffusion follows Fick's first law. The length covered by the diffusing substance is much larger than the diameter d of the grain. The diffusion length is given as $\sqrt{D_g * t}$ where D_g is the diffusion coefficient in the grain and t the time in seconds.

$$d << \sqrt{D_g * t} \qquad (8)$$

Regime B can be described as a transition state between A and C whereas C can be taken as pure grain boundary diffusion. The diffusion mechanism can be interpreted as grain boundary diffusion with conveyance of diffusing substance into the grains. This type of motion can be observed when the conditions for regime A and C are not completely fulfilled. The length covered by the diffusing substance is much shorter than the grain diameter but larger than the width δ of a grain boundary.

$$\delta << \sqrt{D_g * t} << d \qquad (9)$$

When observing a material with very different coefficients for bulk and grain boundary diffusion and when operating on short time scales or at low temperatures regime C is favoured. Motion of matter occurs preferentially along grain boundaries, there is no leakage of matter into the bulk grains. The length of diffusion is vanishing.

$$\sqrt{D_g * t} << \delta \qquad (10)$$

1.2.3) Method of First Arrival (Time Lag Method)

For quantification of diffusion processes in thin film systems, Gupta and Ho introduced an overview of different mathematical possibilities. [28] When investigating diffusion in thin layer systems the layer of diffusant is covered with a layer of diffusion medium. Before the annealing step, the concentration of the diffusing substance on the sample surface and within the bulk diffusion medium is zero. After temperature treatment of the specimen, the diffusant enriches in the diffusion medium and consequently moves toward the surface of the layer system. The so-called time lag or first arrival method utilizes the temperature dependence of a specific diffusant to

appear at the surface of the investigated system. The time period until the analyte appears at the surface is known as the first arrival time t_{fa}.

For taking the right conclusions from the experimental data, some assumptions have to be considered. The occurrence of phase transitions and solid-state reactions interferes with the pure diffusion principles. Additionally, the concentration of diffusant is taken to maintain constant on both, the source-matrix and matrix-recipient interface. This assumption is clearly violated when performing enrichment experiments but however, the enrichment might be negligible if the concentration of the enriching component is low. This experimental setup provides the possibility to simply test the effect of different diffusion barriers on the speed of diffusion. By comparison of diffusion delay times for different temperatures it is possible to develop diffusion models for the observed systems.

When assuming several assumptions, including diffusion to occur in only one direction in space, a mathematical expression for extraction of a species' diffusion constants from first arrival measurements is provided by Crank (formula 10). [29] As some of the mentioned prerequisites are not met in real systems, the obtained numbers for D can only be taken as estimations.

$$D = \frac{x^2}{2 * t_{fa}} \qquad (11)$$

Where x is the layer thickness of the investigated system.

So far, the time lag method has mainly been applied for data obtained with Auger electron spectroscopy (AES). [30] Utilization in ToF-SIMS is comparatively novel and limited to very few examples. [31]

1.2) Applications of ToF-SIMS

1.3.1) Distribution of Light Elements in Micro-alloyed Steels

Steels are multicomponent alloys consisting of iron, carbon and various other elements. During processing, these elements are distributed over the microstructure causing the resulting properties of the material, which makes understanding of elemental contribution an important tool in steel manufacturing. In steels, only a small amount of boron (several ppm) is added during production. By doing so, formation of the bainite phase is promoted whilst the transformation from austenite to ferrite is suppressed. Resulting, the hardenability of the steel is increased. In contrast, a concentration of S and P in a magnitude of several dozen ppm may cause segregation of these elements at grain boundaries leading to an embrittlement at the interfaces. [32]

Figure 8 provides an illustration of the iron-carbon phase diagram. It can be seen that the γ-phase (austenite) starts its transformation to the ductile α-ferrite underneath a temperature of 912° C. However, addition of boron to the system would suppress the resolution of the austenite phase and support appearance of the hard and tough eutectoid bainite phase instead. This non-equilibrium microstructure consists of needle shaped α-Fe (ferrite) crystals with small spherical or ellipsoid crystals of cementite (Fe_3C) nucleating inside the ferrite grains. By formation of bainite phases, residual stresses in steels are reduced leading to an improved material toughness as well as hardenability. [33]

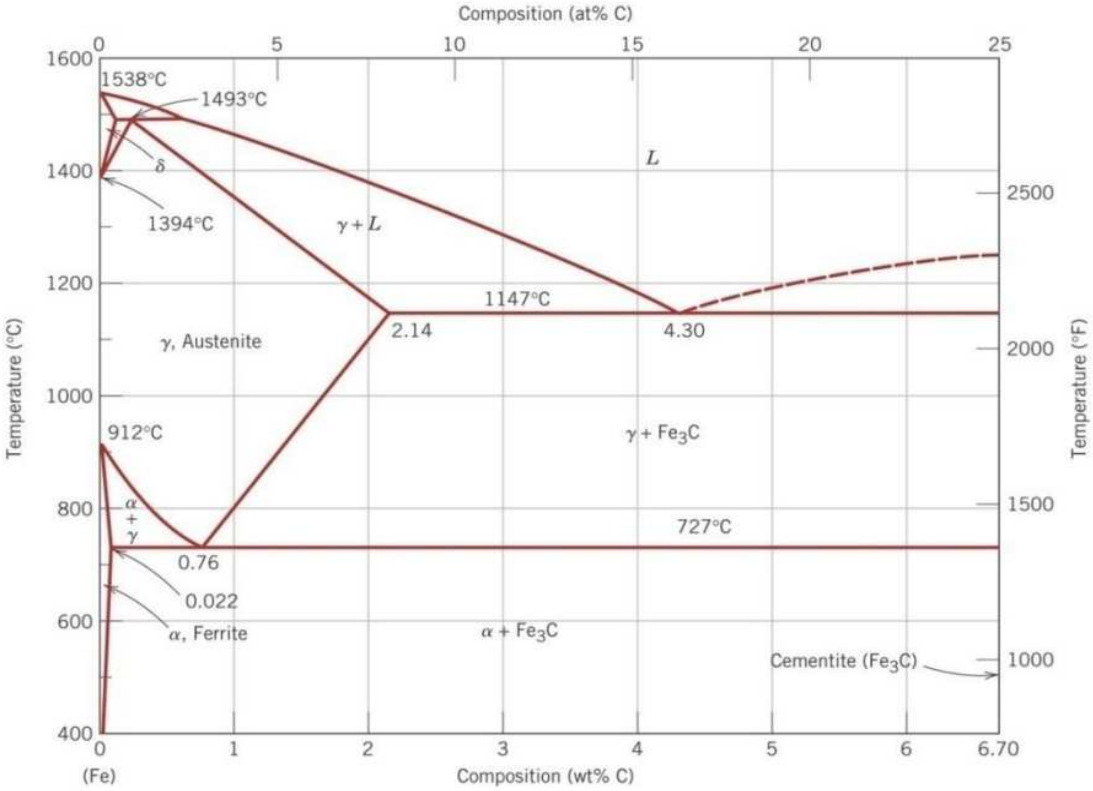

Figure 8: Phase diagram of the Fe-Fe_3C-system: Single-phase regions (L, δ-Fe, γ-Fe, α-Fe and Fe_3C) are separated by two-phase regions by liquidus, solidus or solvus slopes, horizontal lines represent invariant reactions, and addition of boron to steels hinders the formation of α-Fe from γ-Fe and leads to formation of the hard and tough bainite phase (with eutectoid composition).[34]

To assure that boron segregates at the grain boundaries and does not form precipitations like BN, B is alloyed with titanium or niobium that are preferential reacting with carbon and nitrogen to form the corresponding nitrides and carbides. Consequently, boron accumulates at austenite grain boundaries and occupies ferrite nucleation sites inducing a delay in ferrite formation that in turn leads to the mentioned bainite formation.

By use of ToF-SIMS in BA and CBA mode it is possible to perform elemental mapping with a lateral resolution of 200 nm and below. By comparing the high-resolution images produced by ToF-SIMS to scanning electron microscope (SEM) images it is

possible to assign the measured concentrations of boron to any specific component/grain of the materials microstructure and gain information on the connection between the steps of processing and the final properties of the material.

1.3.2) Diffusion Kinetics of isotopically pure ^{41}K in Feldspars

Feldspars are a group of rock-forming tectosilicate minerals representing 41 mass percent of the earths continental crust and are found all over the planet. These minerals have a Vickers hardness of around 800 HV (corresponding to a Mohs Hardness of 6-6.5) and are crystallising either in monoclinic or triclinic crystal lattices. The composition of any feldspar can be described as a transition state between its three natural forms of appearance. These species are the potassium feldspar ($KAlSi_3O_8$), albite ($NaAlSi_3O_8$) and the anorthite endmember ($CaAl_2Si_2O_8$). The number of autonomous states in between these species is illustrated by the isothermal section of the quasi-ternary phase diagram pictured in figure 10. [35]

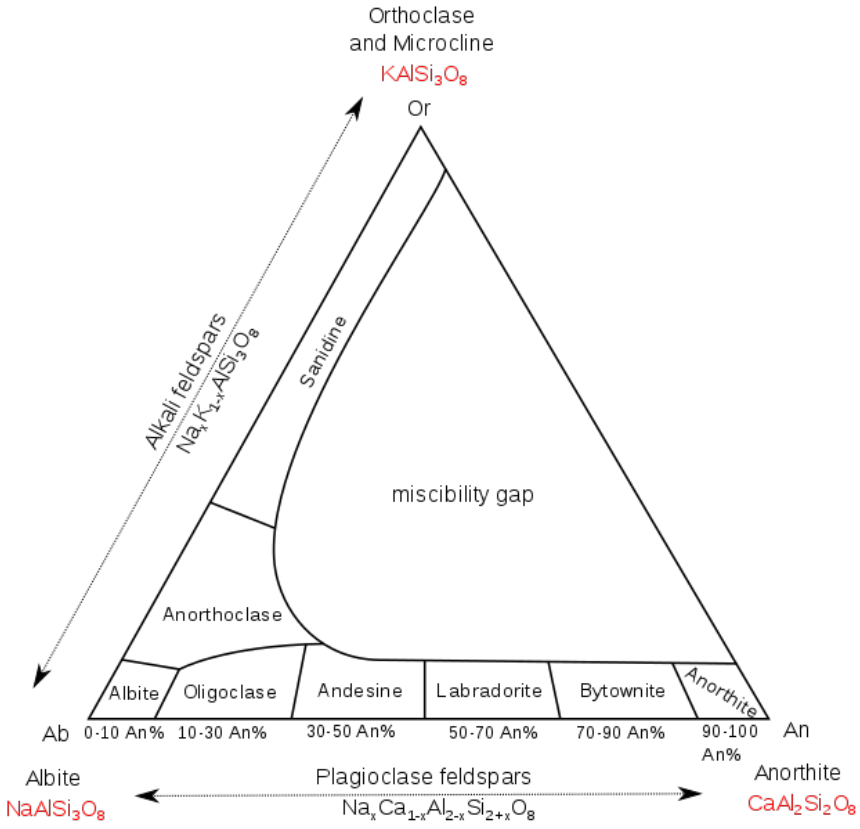

Figure 9: Isothermal section of the quasi-ternary phase diagram of the three feldspar endmembers orthoclase, albite and anorthite. The composition of any feldspar can be described as a transition state between those three endmembers. Source: Wikiwand Feldspar, http://www.wikiwand.com/en/Feldspar, March 22nd 2019.[36]

While solid solutions between albite and orthoclase are called alkali feldspars, all tectosilicates representing mixtures between albite and anorthite are known as plagioclase feldspars. The miscibility between potassium feldspar and anorthite is very limited at ambient conditions. When further decreasing temperature or pressure all alkali and plagioclase feldspars are continuously decomposing to its corresponding endmembers forming a characteristic microstructure. [37] Feldspars are utilized for production of glass and ceramics where the included alumina improves mechanical and chemical resistance of the glass and the alkali metals act as a melting point lowering flux in ceramic manufacturing. In addition, feldspars are employed as a filling material in polymers and paints.[38]

As feldspars appear nearly everywhere, a model for age determination of these minerals would provide the possibility to compare the obtained data of one specific

position with experiments executed in any other country on earth. For age determination of mineral formations, knowledge about the processes of diffusion in the corresponding media is essential. Because of their high coordination numbers, the binding energies of sodium and potassium in feldspars are low leading to a high mobility of these ions comparing to silica and alumina. Due to the structure of feldspars diffusion of alkali ions is favoured in the [101] direction because this direction corresponds to an ion transport channel with sufficient extent to allow diffusion of Na^+ and K^+ threw the crystal planes. This anisotropy of diffusion and the low symmetry of the unit necessitate diffusion measurements in four different crystallographic directions to determine the three dimensional diffusion tensor of the single crystal. By conditioning the surface of a specific site of a homogenous feldspar crystal with an isotopically pure saturated solution of ^{41}KCl and subsequent heat treatment, a distribution – corresponding to Fick's laws of diffusion - of the isotope's concentration over sample depth is reached. When applying ToF-SIMS, utilizing the LMIG in HCBU mode in combination with an oxygen etching beam, it is possible to record depth profiles of the mineral with high mass resolution. By comparison of data collected after different thermal treatments as well as for different crystallographic sites of the specimen it is possible to calculate the diffusion tensor and develop a complete mathematical description for diffusion kinetics in the observed system. [39]

1.3.3) High Temperature Diffusion Kinetics of Al in Metal Layer Systems

In cooperation with a large manufacturer of high-performance microelectronics, investigations on the diffusion behaviour of aluminum in metallic thin layer systems were executed by use of ToF-SIMS. The shematic structure of the investigated systems is illustrated in figure 11.

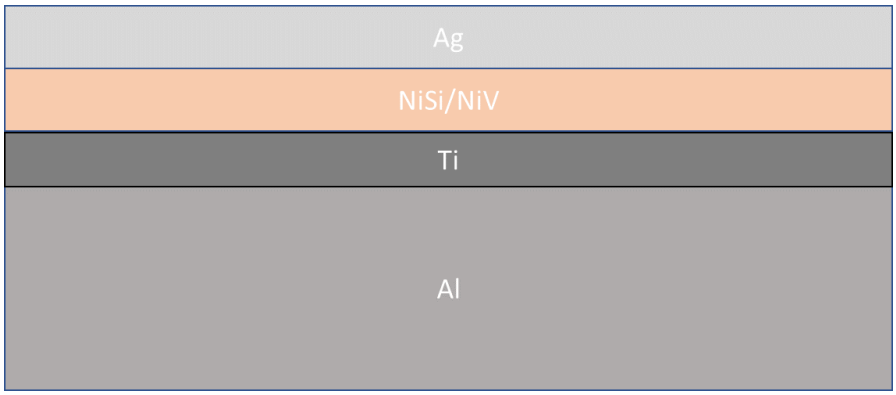

Figure 10: Illustration of the structure of the metal layer systems: The Al seed-layer provides good contact between the metallization system and the substrate, Ti serves as diffusion barrier, NiSi/NiV are solder materials and Ag protects the surface from oxidation. The thickness of the Al layer is magnitudes larger than the other layers thicknesses. Therefore, it is possible to assume that the diffusion equilibrium cannot be reached during the period of the experiment

The sum of the total thicknesses of the three upper layers is about 900 nm while the Al seed-layer is about 3 µm, providing a quasi-endless reservoir of diffusing substance. The Ti layer serves as a diffusion barrier, NiSi or NiV are applied as solder materials and Ag protects the surface from oxidation. Additionally, the samples were treated with different amounts of nitrogen gas during manufacturing, to determine its influence on the diffusivity of Al.

For understanding of diffusion processes, it is usually sufficient to preheat the sample and perform a depth profiling in order to obtain the depth of diffusion into the bulk matrix. However, for multi-layer systems this type of diffusion experiments are not practicable, as the sequence of different layers would result in matrix effects that in turn would hinder successful determination of diffusion constants. The IONTOF ToF.SIMS 5 devices provides special equipment allowing the operator to investigate diffusion in multi-layer systems. The “Heating and Cooling” (H/C) – sample holder enables performance of measurements in the temperature range of -130° C to +600° C with an accuracy of $\pm$ 1 ° C and is described in more detail in section 2.1.1). This setup facilitates a constant diffusion path and the possibility to obtain real diffusion coefficients by monitoring the amount of diffusing element approaching threw the metal layer system.

2) Experimental

2.1) Operating the ToF.SIMS 5

2.1.1) Sample Preparation and Handling

In material science, the type of material investigated as well as the type of information needed vary over a broad range necessitating the supply with special configuration for sample preparation and handling. In the ToF.SIMS 5 these requirements are met by introduction of different sample holders enabling the operator to obtain data within a wide spectrum.

Whenever size and composition of the observed specimen offer the chance, the back-mount sample holder - pictured in figure 12 - is utilized. As its name indicates, the samples are mounted on the backside of the holder. This means that the height of the mounted sample holder is always stable allowing the operator to drive the stage to any position automatically as the geometrical dimensions and consequently limitations of movement are included into the software settings. The position list allows the operator to save any relevant positions and retrieve it at a later point of time. In principle, multiple samples of cross sections of 1*1 cm square can be mounted simultaneously. In the centre of the stage, there is a Faraday Cup for performance of current measurement of the applied ion and electron sources. For calibration of height and further alignment, the stage includes a reference height. By driving the stage upwards manually until the back-mount is just in electrical contact with the extractor and setting the height up to 1.5 mm starting from that point, the reference height is set and saved to the position list. One sample mould is equipped with a silicon waver that is utilized for optimization of the beam guidance as well as dimensions of the applied raster. For performing high spatial resolution measurements in imaging mode, it is necessary to adjust the focus of the LMIG beam.

Therefore, the back-mount sample holder is equipped with two copper grids, the so-called “A-Grid” respectively 1.000 mesh grid that consist of a thin copper net with a specific distance between two wires (250 respectively 1.000 mesh). A capital “A” placed in the centre of the grid simplifies orientation and is eponymous for the element.

As explained, the area for any samples investigated by use of the back-mount sample holder is limited by about 1*1 cm square. When working with larger components it becomes necessary to cut or break them into smaller pieces. Whilst metals might be cut by use of a saw, wafers are broken alongside the crystal planes of the substrate after slitting it slightly with a diamond blade. Any specimens are screwed base from the backside of the holder by use of metal blocks and links. Smaller, thin samples can be stuck to the top of a metal block by use of conductive tape. When operating with any devices or materials integrated into the process of sample and measurement preparations, the operator must wear rubber gloves as any organic residues would trouble the pressure control and subsequently disturb the measurement. The surfaces of resistant materials as metals or some microelectronics are cleaned by use of isopropanol before being mounted into the back-mount holder. However, the standard cleaning procedure for any type of surface is a short flooding with nitrogen gas before introduction to the load lock of the ToF.SIMS 5. In the load lock of the device, a pre-vacuum of about $5*10^{-6}$ mbar is arranged before the sample holder is transferred to the measuring chamber. This procedure of surface cleaning and transfer is the same for any of the sample holders described below.

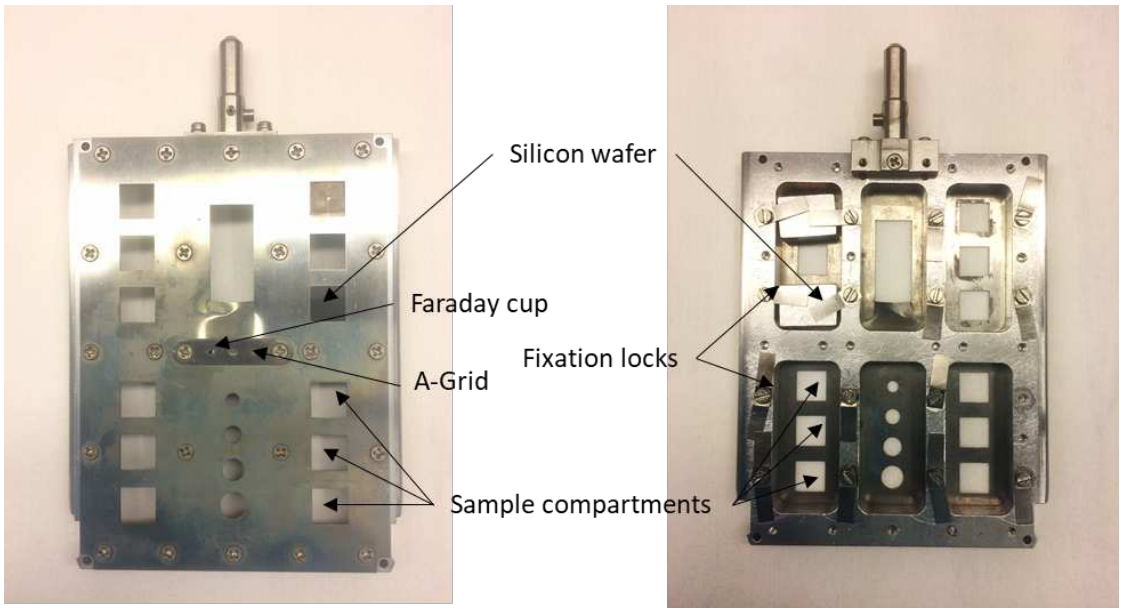

*Figure 11: Picture of the back-mount sample holder utilized in a ToF-SIMS 5 device: All tools that are required for alignment of the ion optical system (Faraday Cup, Si wafer, A-Grid) are included to this sample holder. Application of the back-mount holder is recommended whenever possible. The sample size is limited to 1*1 cm square.*

For samples whose geometrical size is larger than the maximum space provided in the moulds of the back-mount holder IONTOF offers an additional stage for mounting samples with arbitrary dimensions on top. Investigation of a specimen by use of this so-called top-mount holder only pays if either the material cannot be cut or broken without destruction of the interesting surface site or if the sample is embedded in a matrix due to specific requirements for supporting experiments. An image of the top-mount sample holder is provided in figure 13. Metals that are embedded in resins or duroplastic Bakelite materials for surface polishing and subsequent imaging in a scanning electron microscope (SEM) are only one example for specimens necessitating application of the top-mount sample holder. For performing a measurement by use of the top-mount, the analysed sample is stuck on top of the holder by use of conductive carbon tape. After material dependent cleaning of the investigated surface, a short flooding with nitrogen gas is executed for all type of species. Especially for non-metallic materials, the surface of the specimen is conductively linked with the steel surface of the sample holder using adhesive tape persisting of copper to compensate for surface charging due to the sputtering

process. As any sample has its specific geometry and particularly height, the software of the ToF.SIMS 5 device does not allow automatic movement of the stage, because this might lead to a collision in between the specimen and the measuring system, inducing serious damage. Piloting of the stage can only be achieved manually and with permanent surveillance of the sample position in the measuring chamber. In comparison to the back-mount holder, the top-mount does not contain a referenced "A-Grid" and silicon wafer and has no calibrated reference height, as varying sample geometries and complicated movement would hinder alignment anyway. Use of the Faraday Cup is also limited due to the absence of a reference height. This necessitates utilization of the back-mount holder to align the ion optical system before performing any measurements on the top-mount holder. Due to these handicaps in measurement preparation, sample handling and the permanent risk of damaging specimen as well as the ToF-SIMS device application of the top-mount sample holder is only applied when inescapable..

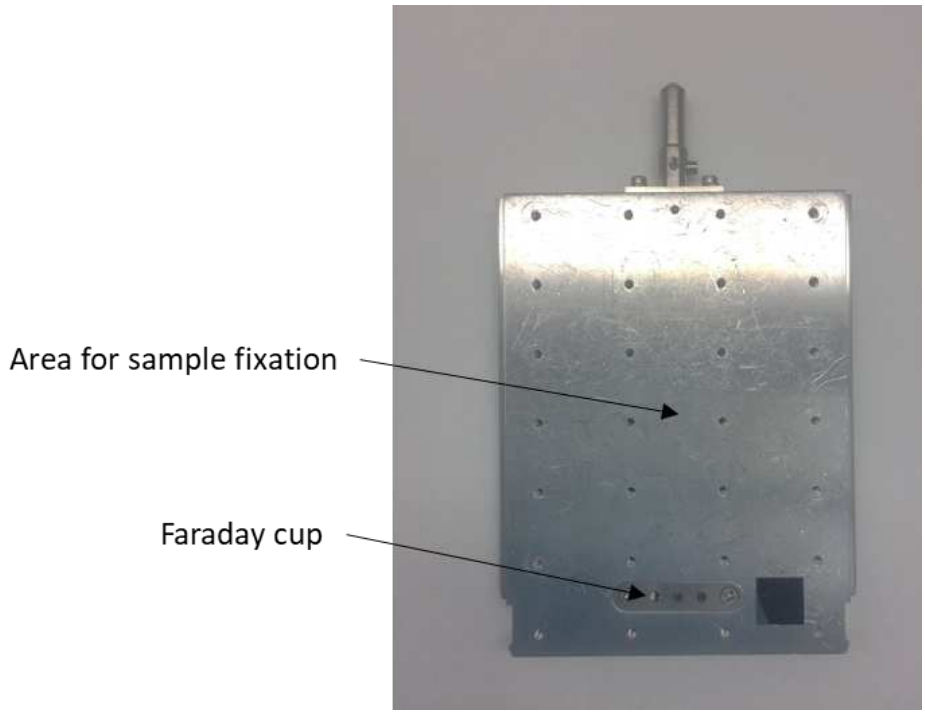

Figure 12: Picture of the top-mount sample holder utilized in a ToF-SIMS 5 device: Samples are stuck on top of the holder by use of conductive tape. The holder provides the possibility of investigating larger samples. Due to restrictions in automatic stage control and a lack of a reference height it is not possible to align the ion optical system by use of the top-mount sample holder.

In addition to the two sample holders described above, the manufacturer provides the so-called “Heating and Cooling” (H/C) holder pictured in figure 14. This sample holder offers the option to perform temperature programmed SIMS. It enables the operator to set the temperature of the specimen inside the measuring chamber to a specific temperature or even run a temperature program including several heating and cooling events as well as phases of constant temperature. The investigated specimen plate or wafer is cut to a size of 1*1.4 cm and mounted on top of a copper block by placing it underneath a metallic frame that is in turn fixed with four screws. By carefully placing the included thermocouple in between frame and surface of the sample, the system is enabled to measure the temperature at that point. Heating as well as cooling of the sample is performed by a thermal link between the copper block on the bottom of the specimen and an elevated cooling finger as well as a resistive heating system. The cooling finger in turn connects to a copper bar linking to a supply of liquid nitrogen, as the height of the stage is set when preparing for the measurement. To achieve maximum temperature accuracy heating and cooling system are always operating against each other offering the possibility to perform measurements in a temperature range between -130° C and +600° C with a precision of $\pm$ 1° C.

Similar to the top-mount sample holder, the H/C-stage does not contain a reference height, Si wafer and “A-Grid”. Also, the manufacturer relinquished on a Faraday Cup for practical reasons. Therefor application of the back-mount sample holder is required in preparation for any temperature programmed SIMS measurements. The H/C-stage provides space for only one specimen at once as is limited to only one cooling and heating system. Hence, measuring time is increased, as steps of transfer and sample preparation must be executed after any single measurement. In addition, the repeatability for any analysis strongly depends on the careful and consistent identical placement of the thermocouple in between the surface of the investigated sample and the metallic fixation frame. Otherwise, there might be a gap between the surface of the sample and the junction dot of the thermocouple. Consequently, the actual temperature at the surface of the specimen would exceed the measured

temperature clearly due to the restricted temperature transfer under conditions of ultra-high vacuum.

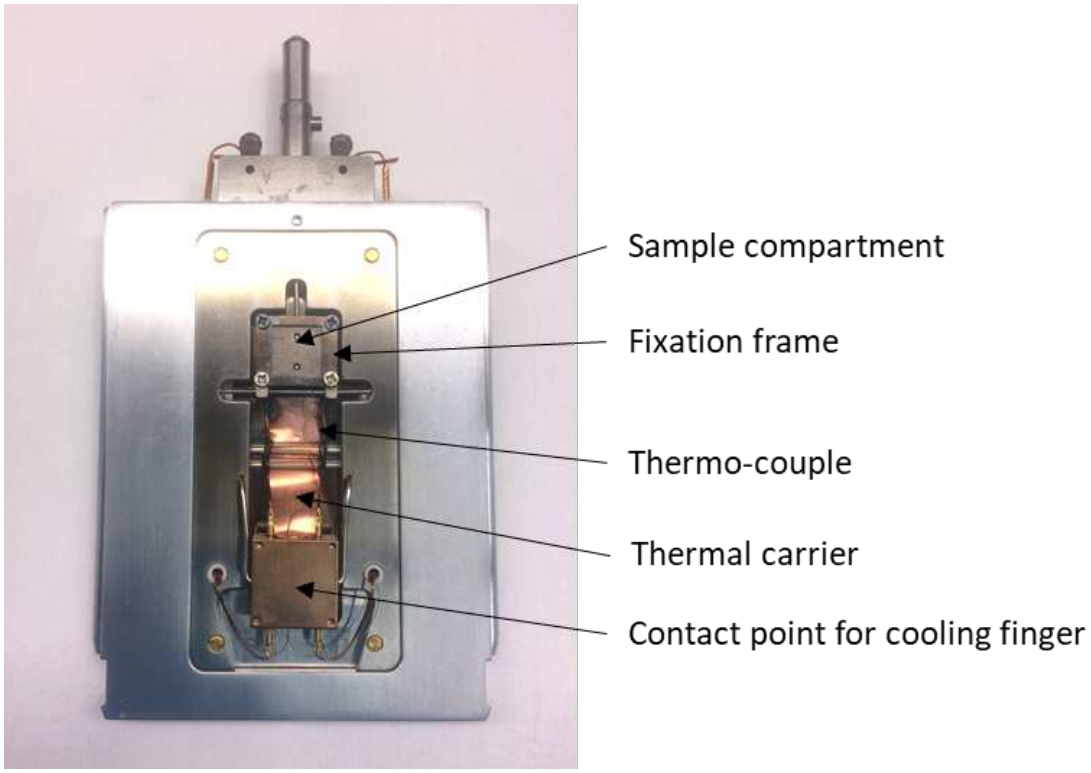

*Figure 13: Picture of the "Heating and Cooling" (H/C) sample holder utilized in a ToF-SIMS 5 device: The sample of size 1*1.4 cm is fixed underneath a metallic frame by use of four screws, a thermocouple is placed in between sample surface and frame before fixation. The metal block underneath the sample is thermally linked to a resistive heating system as well as a contact point to a cooling finger that in turn is connected to a reservoir of liquid nitrogen. The holder allows temperature programmed SIMS measurements in a region of -130° C to +600° C but is limited to investigation of one sample at one time.*

2.1.2) Alignment of the ToF.SIMS 5

Schematic illustrations of the beam forming compounds for the ion optical system of the DSC as well as the LMIG are provided in figures 15 and 16. Before starting the beam alignment of the IONTOF ToF.SIMS 5 the power supply for the analyser unit, the LMIG as well as the employed sputter gun are turned on. The lastly saved adjustments for the measuring gun and DSC are loaded and the emitters and ion optics are initialised. The warm-up time of the 25 keV Bi emitter of the LMIG and the Cs emitter of the dual source column is about thirty minutes offering enough time to prepare the samples. When using the gas source of the DSC, a warm-up is not

necessary, but it is required to regulate the pressure at the ionisation filament by tuning the flow of the gas in use. All beam alignments are performed on the back-mount sample stage because it includes some essential features missing on the other stages (A-Grid, Reference Height, Si-Wafer). When the emission current of the LMIG is stable at a value of 0.8 µA and the sample is loaded, the stage is moved to the "Faraday Cup" position where measurements of the final beam currents of both guns are carried out. For current measurements, the instrument setup is always adjusted to positive ion mode. The LMIG current is optimized by centring the beam at apertures 1 and 2 followed by regulation of the set values for X- and Y-blanking and varying the voltage applied to lens source. The aspired value for the current strongly depends on the mode of operation (table 1). For increasing the sputter gun current the settings for X- and Y-crossover in the focus slide of the DSC menu are shifted. When working with a gas source, variation of the beams static deflection may additionally lead to an improved intensity. After sufficient adjustment of the current the setup for flood gun and analyser unit are loaded and the mode of ionization is altered to the required charge (positive or negative).

Next, the stage is driven to the position of the reference height, allowing the operator to optimize the height with respect to the analyser unit. This is reached by pulsing the LMIG onto the surface and monitoring the resulting secondary ion image in the Navigator field. After pressing the button for "Reference Circle" the image of the total area is replaced by a circle with a diagonal of about 100 µm appearing near the centre of the image field. By ticking the box next to the "Finetuning" option in the analyser menu and subsequent adjustment of parameters X and Y in the TOF slide the circle is centred to the field of view as exactly as possible. Now the stage is manually driven to an undamaged area on the silicon waver that is on a fixed position in the back-mount sample stage. The height of the sample is adjusted by pressing the "Reference Circle" button once again and ensuing centring the circle by manually tuning the sample height z. Afterwards the field of view in the Navigator is set to 20*20 µm and the pulse length of the LMIG is maximised in the gun slide of the LMIG menu. As soon as a small crater appears on the video image of the surface, the measuring gun is again set to short pulses and the field of view is increased to its maximum value again.

Next, the crater is centred by moving the stage. The secondary ion image and the image taken by the camera are synchronized to each other by adjusting X- and Y-Target in the raster field of the LMIG menu. Analog the beam of the sputter gun is set to an extent of 0 µm to get the smallest accessible spot size and is also centred to the field of view by shifting X- and Y- Target in the raster slide of the DSC menu. To optimize the position and properties of the final measuring beam all steps explained above are iteratively repeated for advanced performance. When performing depth profiling, the size of the raster applied on the DSC is set to a value 200 µm larger than the area of the LMIG raster to avoid crater effects that would complicate evaluation of data.

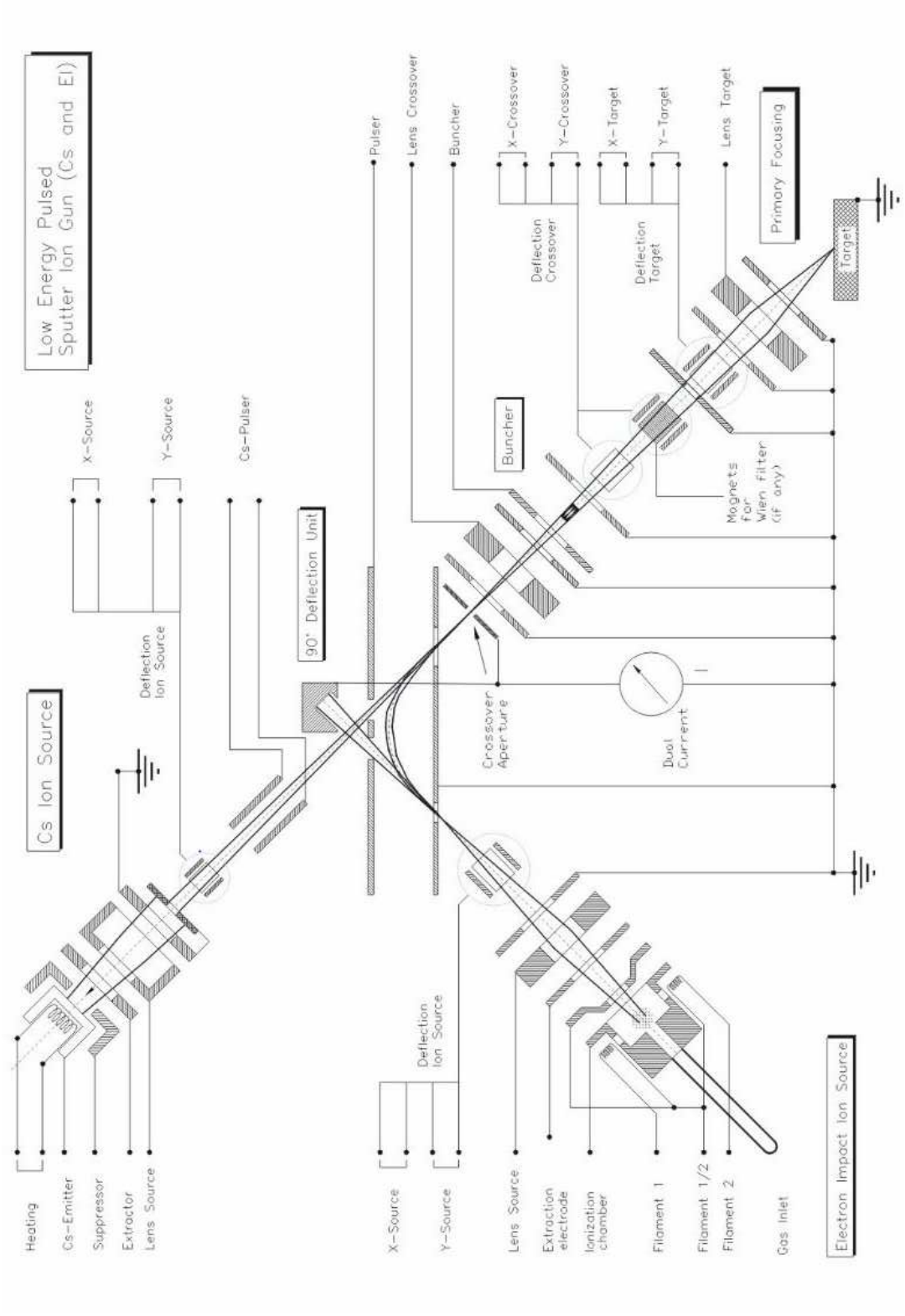

Figure 14: Schematic of all components included into the ion optical system of the DSC: When performing a beam alignment, one tries to tune all values starting with those next to the emitter downwards until the current measured at the Faraday cup is optimized.

When operating measurements in BA or CBA mode adjustment of the Focus and Stigmators of the LMIG is essential. After performing the fundamental alignment, the stage is driven to the position of the A-Grid. There, height is adjusted manually by synchronising the secondary ion image with the image taken by the camera. Following, the flood gun is turned off, the detector in Navigator is switched from SI (secondary ions) to SE (secondary electrons) and the pulse duration of the LMIG is again turned to its maximum value. Now, the SE gain of the detector is set to a value between 6.000 and 7.000 and an image of the copper grid appears on the detector field. For optimization of the focus it is necessary to adjust the beam in a field of view similar to the size of the field in the intended measurement and to resolve structures in the same range of magnitude. Therefore, the stage is manually driven to a position of the grid that was already partially destroyed by previous ion bombardment. The number of pixels per image applied depends on the size of the field of view: As the spot size in BA is about 200 nm the maximum resolution for a field of view of 50*50 µm is reached with 256*256 pixels. By iterative tuning of the parameters Lens Target and X- and Y- Stigmator, the resolution of the SE image is optimized. Again, for an ideal alignment all steps, including centring of the acceptance circle at the reference height and regulation of the beam position on the Si wafer are repeated until a constant guidance is achieved.

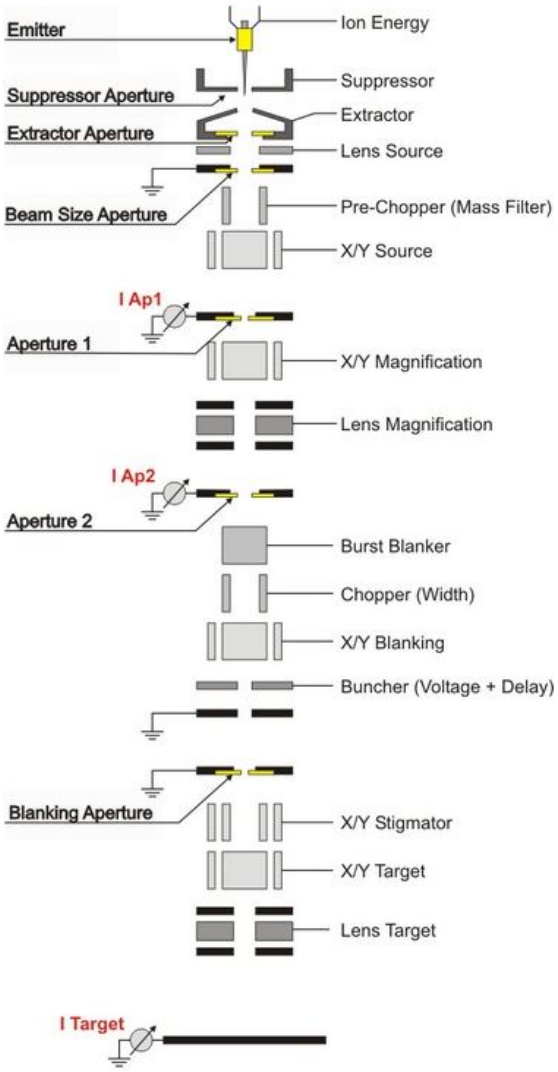

Figure 15: Illustration of the components of the ion optical system of the LMIG: By changing the voltages applied to the three magnetic lenses the position of the crossover point(s) can be tuned. Size and shape of the impacting beam are varied by tuning of other beam forming compartments.

After opening the three programs for evaluation of data taken by Tof-SIMS (mass spectrum, depth profiling, imaging) in the F-Panel, the stage is driven to the position of the investigated sample. There, the height is adjusted by use of the acceptance circle and the secondary ion image is stopped. After calibration of the recorded mass spectrum, the operator is able to enter the required conditions and run the measurement. Usually, when aligning new compounds of the ToF.SIMS 5 the whole adjustment process might take longer but generally remains unchanged.

2.2) Applications

2.2.1) Distribution of Light Elements in Micro-alloyed Steels

In cooperation with a large manufacturer of high performance steels investigations on the distribution and segregation of boron in steel were executed in order to develop an imaging mode for high resolution elemental mapping in the ppm region. Therefore, steel samples were embedded in a thermoset Bakelite matrix and their cross sections were grinded and polished to a grain size of 1 µm and consequently etched by use of Nital (HNO_3 in EtOH). The idea was to mark a region on the interface of metal and matrix by sputtering a frame by use of the LMIG and subsequently taking images with ToF-SIMS in BA mode and SEM from that specific area. By comparison of the elemental distribution maps to the pictures obtained in the electron microscope assignment of elemental segregation to corresponding elements of the materials microstructure were performed.

As the investigated samples were embedded in order to perform SEM measurements utilization of the back-mount sample holder was precluded. Alternatively, the samples were stuck on the top-mount holder with conductive tape and the surface of the specimen was put in conductive contact with the sample holder by use of adhesive copper tape. Prior to introduction into the measuring chamber, the metal surfaces were cleaned with isopropanol and following flooded with nitrogen gas. As the top-mount sample holder does not contain a reference height, silicon wafer and "A-Grid", application of the back-mount is essential for aligning the ion optical system before starting measurements on the embedded samples.

As the sputter yield for boron is not sufficient to perform measurements in the aspired concentration region of ppm it was decided to employ the ToF-SIMS in its negative operation mode utilizing the Cs^+ source of the DSC to monitor and compare the concentrations of different boron oxides. After setting the measurement height, the area of particular interest was cleaned by application of the sputter gun with its raster size set to a value of 1000 µm square for 3 seconds in order to achieve constant conditions. For optimization of the resolution the field of view relevant for the 2D ToF-SIMS images was set to 50*50 µm square. Starting at the interface several

squares of that size were set one above the other to obtain a stepwise profile of the region of interest. An illustration of the specimen and measurement setup is provided in figure 17. By manual post-processing of the obtained images, their explanatory power and the chances for effective assignment to corresponding microstructural phases was greatly enhanced.

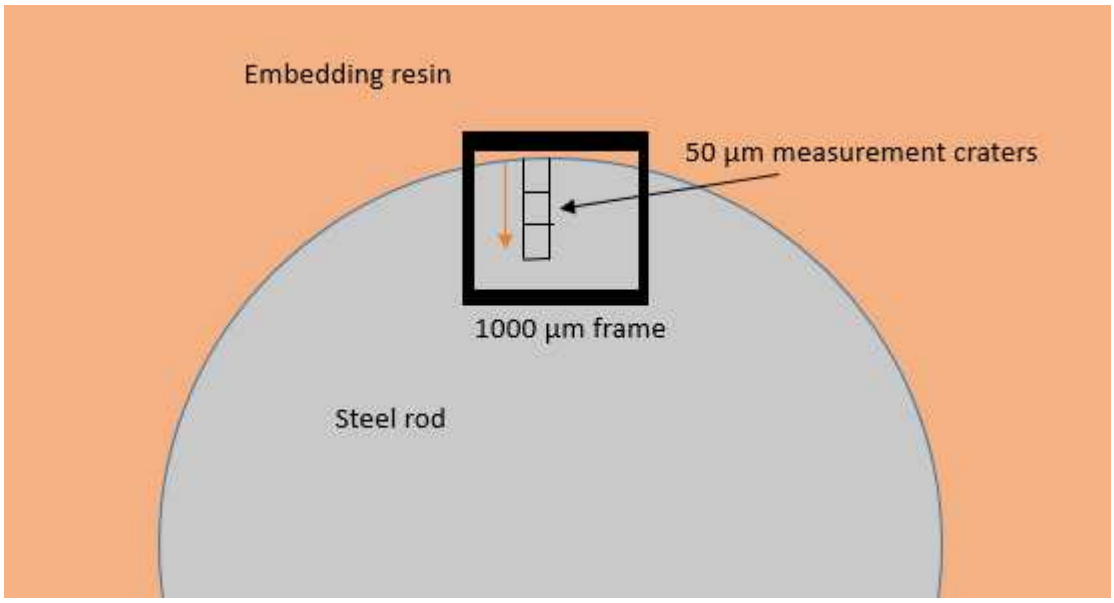

Figure 16: Schematic illustration of the experimental setup: The steel rod was cross sectional embedded in a Bakelite matrix and subsequently grinded and polished, to mark a specific region. A 1000 µm frame was sputtered onto the rim region by use of the LMIG in DC mode in order to mark the field of interest. For stepwise depth profiling several craters of 50 µm square were set one upon the other on a noticeable spot within the frame.

2.2.2) Diffusion Kinetics of isotopically pure 41K in Feldspars

For implementation of a method for age determination and understanding of the mechanisms of rock formation, the diffusion of isotopically pure ^{41}K in feldspars of different composition and temperature treatment was investigated in cooperation with the department of lithosphere research at the institute of geology (Uni Wien). The mineral materials were cut at the institute of geology corresponding to the orientation of the feldspar crystals into pieces of approximately 2*2 mm square and 1 mm height. After covering it with a solution of saturated ^{41}KCl and subsequent heat treatment, the site of interest was marked by slightly slitting it with a scalpel.

Following the samples were transferred to the institute of chemical technologies and analytics (TU Wien) where ToF-SIMS measurements were performed in positive ion mode with CBA beam guidance. The device was operated in CBA mode due to two advantages when comparing to HCBU mode. On the one hand, the representation of the isotope ratio is more reliable in CBA ^{40} and on the other hand, the high intensity of secondary ions generated in HCBU would exceed the dynamic range of the detection unit when investigating K-feldspars. The mineral pieces were carefully stuck to metal blocks, mounted to the back-mount sample stage by use of conductive tape and flooded with nitrogen gas prior to introduction into the measuring device. As the specimens are non-conductive the pause time between an etching and a measuring pulse was increased additive to application of the flood gun. Additionally, the mode of rastering the surface was altered from sawtooth to random to avoid occurrence of different excitation processes right next to each other within a short period of time. The reason for these provisions is the obviation of surface charging that would lead to an increased background signal. For depth profiling of positive ions the oxygen emitter of the dual source column was applied. The measurements were performed until the concentration of ^{41}K reached the magnitude of its natural relative frequency. The depth of the crater was determined by use of a Bruker DektakXT Stylus Profiler. The measured depth profiles were subsequently calibrated to the obtained values. All data collected was delivered to Rainer Abart at the institute of geology (Uni Wien) for further calculations.

2.2.3) High Temperature Diffusion Kinetics of Al in Metal Layer Systems

For understanding of the mechanisms behind the diffusion of aluminium in microelectronics, various metal layer systems were investigated by use of ToF- SIMS in HCBU mode. The specimens differed in layer setup as well as content of nitrogen. For determination of the diffusion constants of these systems, all independent measurements were performed under different temperature conditions, in the range

of 500 to 550 °C, by use of the “Heating and Cooling” sample holder. Therefore, the wafers were broken into pieces of 1*1.4 cm and one after the other fixed underneath the metallic frame of the holder with the thermocouple carefully placed in between sample surface and frame. To ensure that all measurements are comparable to each other, placement of the thermocouple as well as fixing of the metallic frame was executed identically each time. The surface of each sample was flooded with nitrogen gas prior to introduction into the measurement chamber. As the H/C-stage does not contain a Faraday Cup, Reference Height and silicon wafer, alignment of the HCBU mode has to be performed on the back-mount holder before starting the measurements. The reservoir for liquid nitrogen at the back of the ToF.SIMS 5 device has to be filled in order to achieve maximum temperature accuracy. After some hours the filling level of the reservoir should be checked and restocked to guarantee constant operation conditions. After introduction of the sample into the measuring chamber and subsequent adjustment of height and area of interest, the surface was prepared by pre-sputtering an area of 1000*1000 µm with the oxygen source of the DSC for three seconds to remove surface contaminations and obtain defined starting conditions. Following, a 300*300 µm 2D measurement, meaning that only the LMIG is applied, was performed in positive ion mode. The temperature of the H/C-stage was set to the desired value and the concentration profile of the surface is recorded. Each measurement was stopped as soon as the concentration of Al reaches a constant value. Evaluation of data was executed by use of first arrival methods described in the introduction.

2.3) Additional Techniques

2.3.1) Scanning Electron Microscopy (SEM)

For assigning of different phases within the microstructure of micro-alloyed steels to high resolution elemental distribution maps obtained with the ToF.SIMS 5 the observed areas were marked and subsequently measured in a 30 kV FEI Quanta 250 FEG (field emission gun) – SEM at USTEM (service facility for electron microscopy at TU Wien). For labelling of the pictured area, a frame of 500*500 µm was sputtered around the area of interest by use of the LMIG in direct current mode. The applied FEG provides a maximum spatial resolution of 1.2 nm when operated under the condition of high vacuum. All SEM images illustrated in this work were provided by Daniela Wipp from the Institute of Materials Science and Technology (TU Wien).

2.3.2) Profiler

For determination of the depth of craters generated in ToF-SIMS experiments utilization of a so-called profiler is required. The DektatXT Stylus Profiler manufactured by Bruker offers improved repeatability, depth accuracy as well as fast data collection and analysis. For obtaining information on the topography of a specific sample the tip of a diamond needle (stylus) is drawn along a surface constantly measuring the deflection of the tip with an accuracy in the low nanometre region (< 10 nm). Prior to perform a measurement, the planeness of the experimental setup is adjusted manually. For determination of a profile, the stage is driven to two specific points with the region of interest, in our case the sputter crater, lying in the area between those spots by use of the integrated camera. These points are saved to the software that subsequently is asked to perform a line scan in between those points. To make sure, that the baseline is set correctly, the length of the line scan exceeds the size of the crater for some hundred micrometres on both sides. The accuracy of the obtained data depends on the drawing speed of the needle and the settings for total effective range of the profiler. For increasing the quality of data, two line-scans

- each perpendicular to the crater length and perpendicular to each other - are performed for any single crater. The arithmetic mean was calculated to define a single value for the depth of any crater. After two-point linear baseline calibration to set the surface zero, the depth of the crater can be determined by use of the attached software Vision64. To avoid disturbances by crater effects it is necessary to centre the measuring bar using the extent of the analysis beam for depth recording. [41]

3) Results and Discussion

3.1) Distribution of Light Elements in Micro-alloyed Steels

For providing a model to describe the microscopic mechanisms behind the formation of micro-alloyed steels, the boron distribution in the surface region of the cross-sectional prepared samples was recorded by use of the ToF-SIMS in BA mode. Although the spatial resolution in BA mode is poorer than in CBA, comparison of the two modes clarified that resolution in BA is sufficient for identification of individual grains. In addition, the reduced beam intensity in CBA leads to increased measurement times, extending the probability for sample drift during the experiment that in turn leads to a decrease in scientific significance. Due to the bad sputter yield of boron plus its very low concentration in the ppm region, it was not possible to perform the imaging in positive ion mode. Instead, the distribution of different boron oxides was monitored by application of the analyser in negative ion mode. The primary idea was to utilize oxygen ions for etching and by doing so introduce enough oxygen to convert all boron particles into their corresponding oxides. However, comparison of pre-etching of the sample surface by either the oxygen gas source or Cs surface ionisation source illustrated that the amount of oxygen in the sample is sufficient anyway and the relative intensities are higher when sputtering with

caesium ions. As the idea was to compare several distribution curves in dependence of their distance to the surface, several craters of 50 µm square where set one upon the other to cover the total region of interest. Also starting at the rim simplified positioning of the sample as well as relocating the spot when transferring the sample between SIMS and SEM. To maximise the chance for a correct assignment with the images taken by FEG-SEM, it was tried to pick a recognisable spot within the 1000 µm square frame and record any area of measurement with a screenshot.

As the investigated steel rods also contain aluminum in the region of ~0.03 wt%, recording of the distribution of boron oxides is disturbed. Due to the decrease of mass resolution to unity the peaks of BO^- and Al^- cannot be separated, as both ions have a nominal mass of 27 g/mol. The same difficulties occur for $BO2^-$ and AlO^- (M = 43 g/mol) and so on. Therefore, it was decided to monitor the distribution of oxides of the ^{10}B isotope with a natural frequency of 19.6 %. To assure that the measured peak only corresponds to the ^{10}BO- signal, a HCBU measurement of the sample area was performed in addition to the imaging implementation. This problem is illustrated in figures 18 and 19.

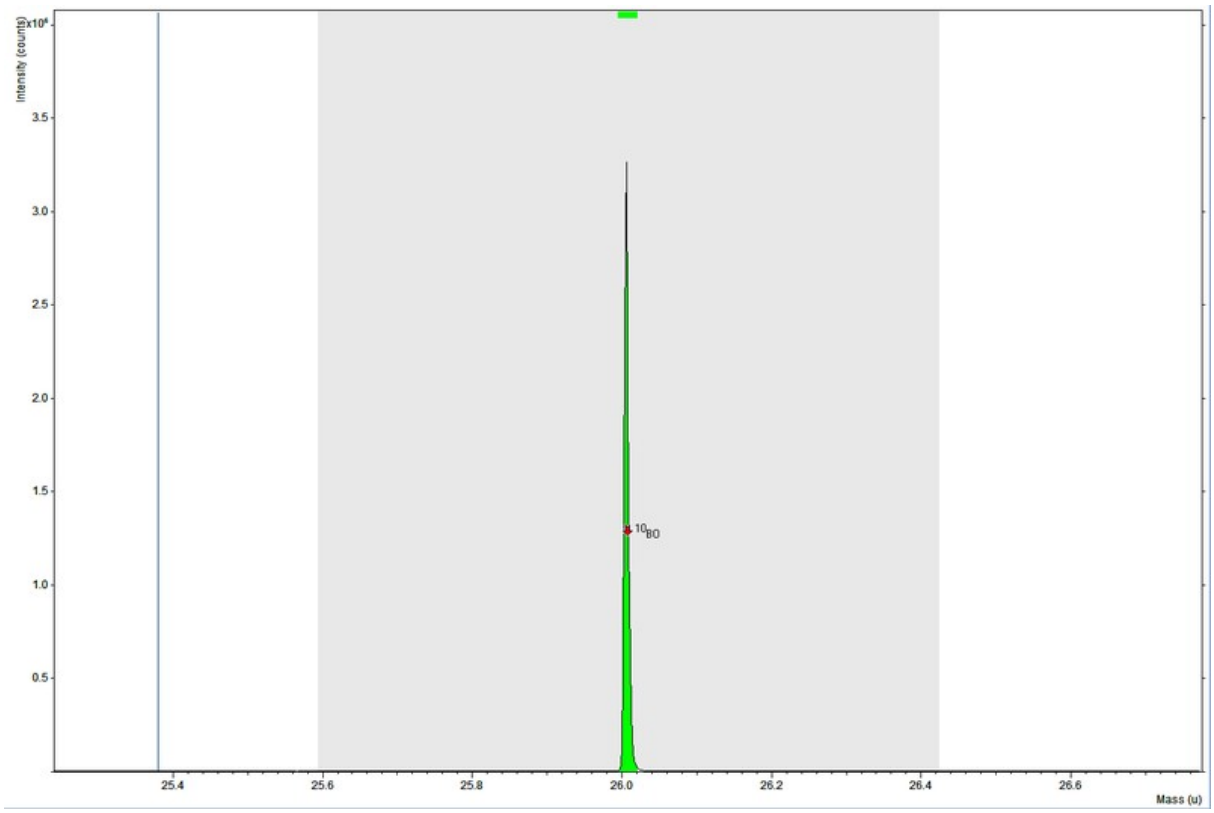

Figure 17: Mass-spectrum of sample 1-1 taken in HCBU mode: The appearance of only the $^{10}BO^-$ signal in the mass range of 25 $\pm$ 0.5 g/mol enables analytical utilization of that peak for imaging applications (BA, CBA) where mass resolution is reduced to unity.

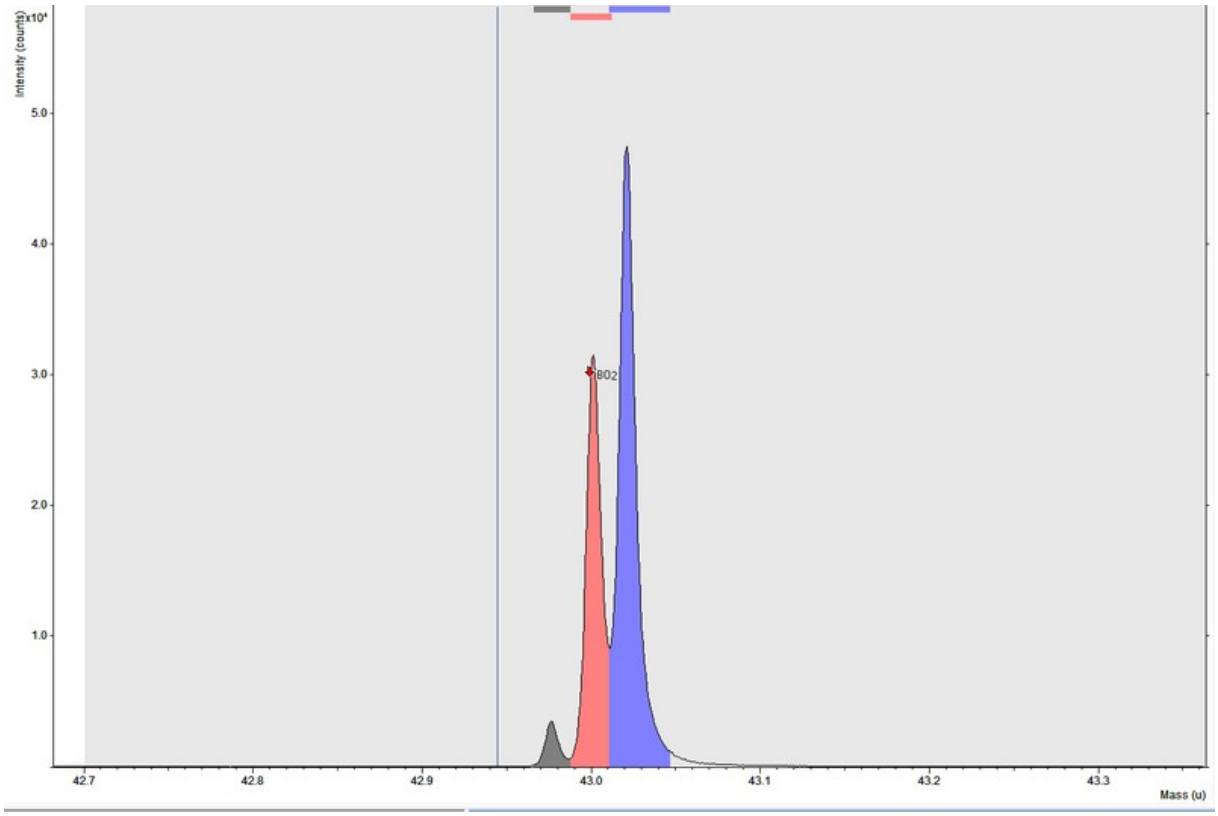

Figure 18: Mass-spectrum of sample 1-1 taken in HCBU mode: Analytical utilization of oxides of the ^{11}B isotope for imaging applications are limited as several peaks of similar nominal mass are recorded for any oxide. The content of alumina within the steels wires leads to falsified results as Al has the same nominal mass as ^{11}BO, AlO has the same mass as $^{11}BO_2$ and so on. In the spectrum above, the grey peak corresponds to AlO^-, while the orange one corresponds to $^{11}BO_2^-$. The blue peak presumably corresponds to traces of organic contaminations (probably $C2H3O^-$).

All images were post-processed by use of the IONTOF software package. By tuning the number of independent pixels as well as the intensity region displayed, the pictures were optimised in order to obtain grains of the microstructure with highest possible resolution. For any of the 50 µm images recorded by use of ToF-SIMS an image with similar size and magnification of the same field of view was taken with a 30 kV FEI Quanta 250 FEG-SEM at USTEM (TU Vienna). By careful comparison of the magnified images generated with the two different methods assignment of elemental distribution to their corresponding phases in the samples' microstructure was performed (figures 21 to 30).

The following figure illustrates the difficulties occurring during BA measurements when monitoring ^{11}B-oxides. Due to the decreased mass resolution, it is not possible

to differentiate between species of same nominal mass, as AlO^- and $^{11}BO_2^-$, AlO_2^- and $^{11}BO_3^-$ and so on. Mass resolution could be increased by application of burst mode but the concentration of boron in the region of ppm would only allow further reduction of intensity for the cost of excessive measurement durations that in turn lead to shifts due to sample drift. Values for measurement conditions are illustrated in table 3.

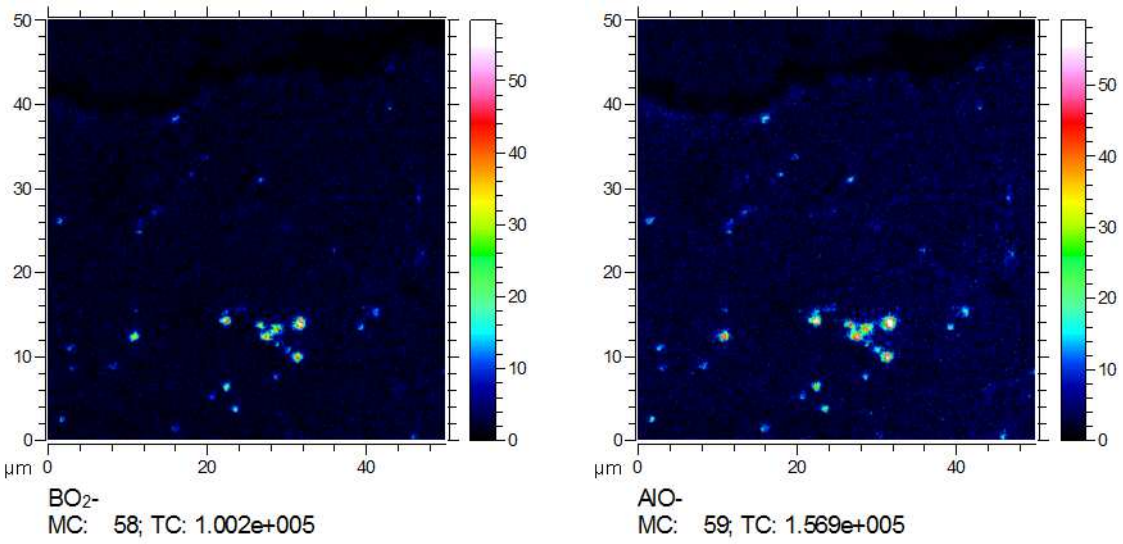

Figure 19: ToF-SIMS images of $^{11}BO_2^-$ and AlO^- of the same sample area indicating that differentiation between the two species is not possible due to the reduced mass resolution when operating the device in BA mode.

		Energy	Crater Size
LMIG	*Bi+*	*25 keV*	*50 * 50 µm*
DSC	*O2*	*2 keV*	*1000 * 1000 µm*
Raster Mode	*random*		
Cycle Time	*45 µs*		
Pixels	*512 * 512*		
Interlaced Mode			

Table 2: Standard operation conditions for ToF-SIMS measurements connected to imaging applications for understanding of the distribution and segregation of boron in micro-alloyed steels

As mentioned above, five measurements with an area of 50 µm square were set one upon each other starting at the rim of the steel wire to develop a stepwise depth profile. In the following, an illustration of five consecutive measurements for a single sample is provided. All five data points contain one secondary ion image of $^{10}BO^-$ taken by ToF-SIMS and one secondary electron image of the microstructure from the same sample position recorded with a FEG-SEM. In addition, a screenshot taken while performing SIMS measurements indicates the measurement position relative to the frame sputtered by use of the LMIG is appended. The screenshot also contains a secondary ion image of the field of view on the left and the current measurement position relative to the back-mount sample holder.

By comparison of the images taken with the two different devices, it was possible to assign grains of the microstructure to a corresponding concentration of boron and gain understanding on the mechanism of segregation. It is clear that B preferentially segregates in those grains exhibiting a light colour in the SEM images. These are grains of pearlite, where formation of lamellar cementite occurred within a ferrite matrix. The dark grains are grains of ferrite only and hardly contain boron. For easier understanding, significant grains and positions were marked with yellow circles, enrichments with red circles. With increasing depth (distance from the rim) the amount of perlitic grains increases whereas ferrite is preferentially formed at the surface of the sample.

Measurement 1

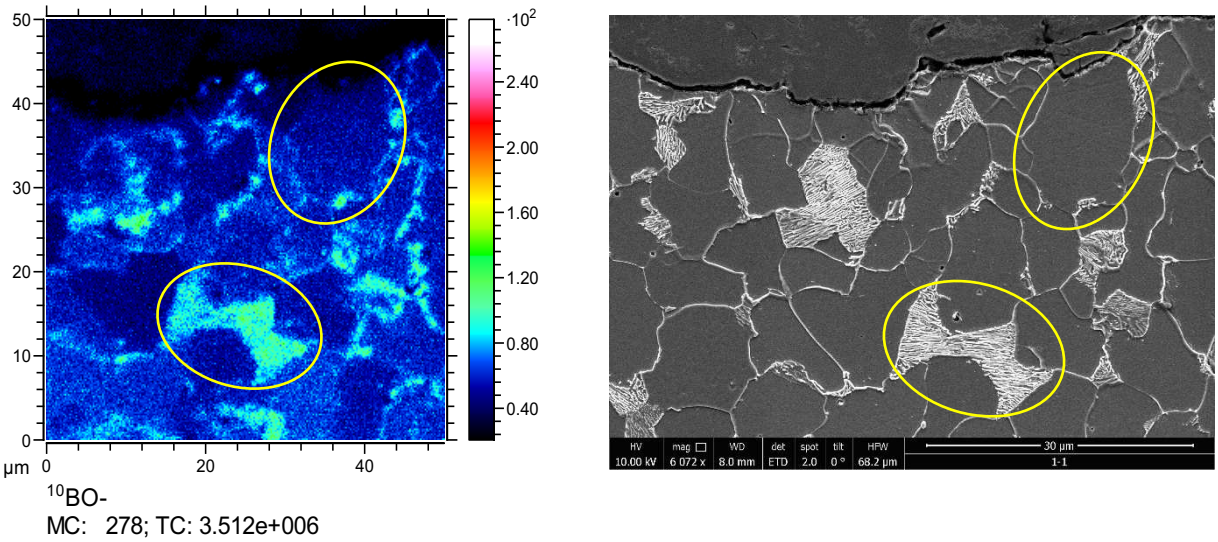

Figure 21: Assignment of elemental maps of $^{11}BO^-$ obtained by use of ToF-SIMS (left) to corresponding phases of microstructures displayed by use of FEG-SEM (right).

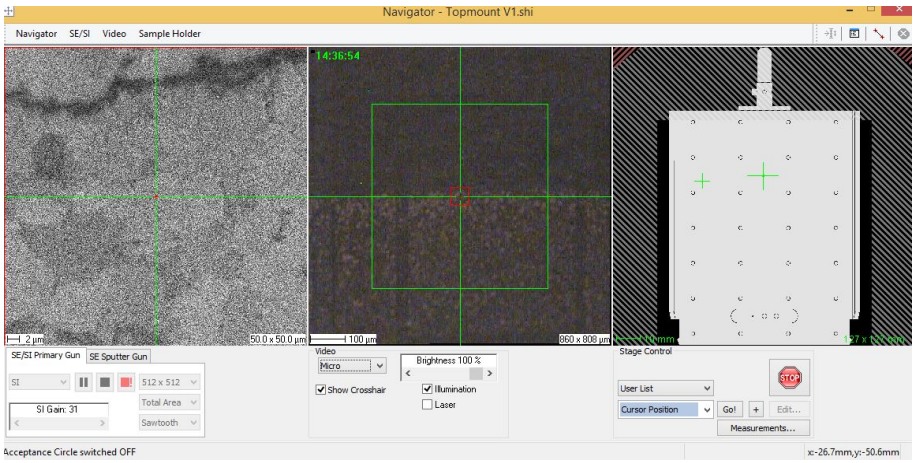

Figure 22: Screenshot of the measurements position of ToF-SIMS: The secondary ion image on the left shows the field of view including grain boundaries. In the centre, an image of the position of the field of view in relation to the pre-sputtered frame is provided. The picture in the right shows the position of the measurement in relation to the sample holder position.

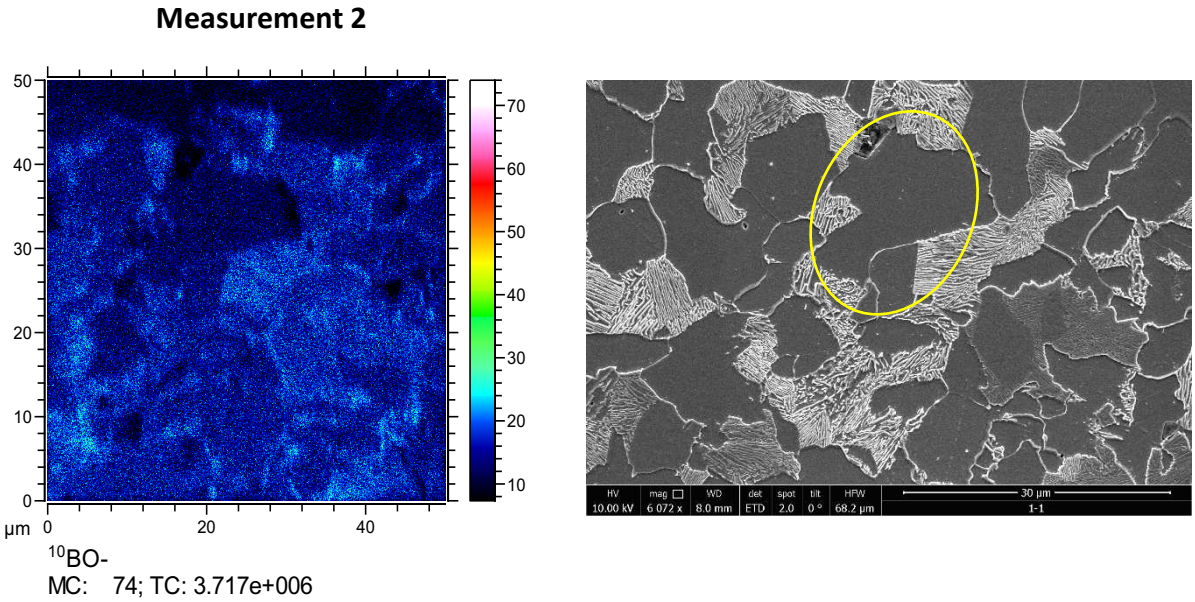

Figure 20: Assignment of elemental maps obtained by use of ToF-SIMS (left) to corresponding phases of microstructures displayed by use of FEG-SEM (right).

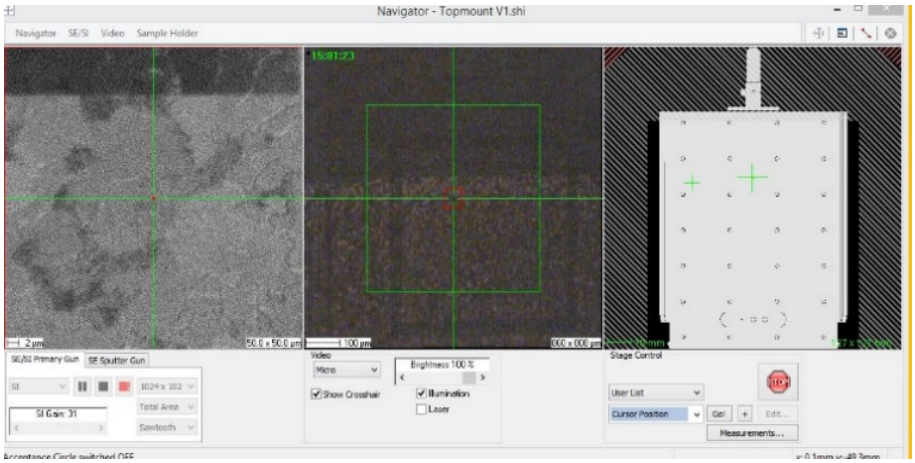

Figure 21: Screenshot of the measurements position of ToF-SIMS: The secondary ion image on the left shows the field of view including grain boundaries. In the centre, an image of the position of the field of view in relation to the pre-sputtered frame is provided. The picture in the right shows the position of the measurement in relation to the sample holder position.

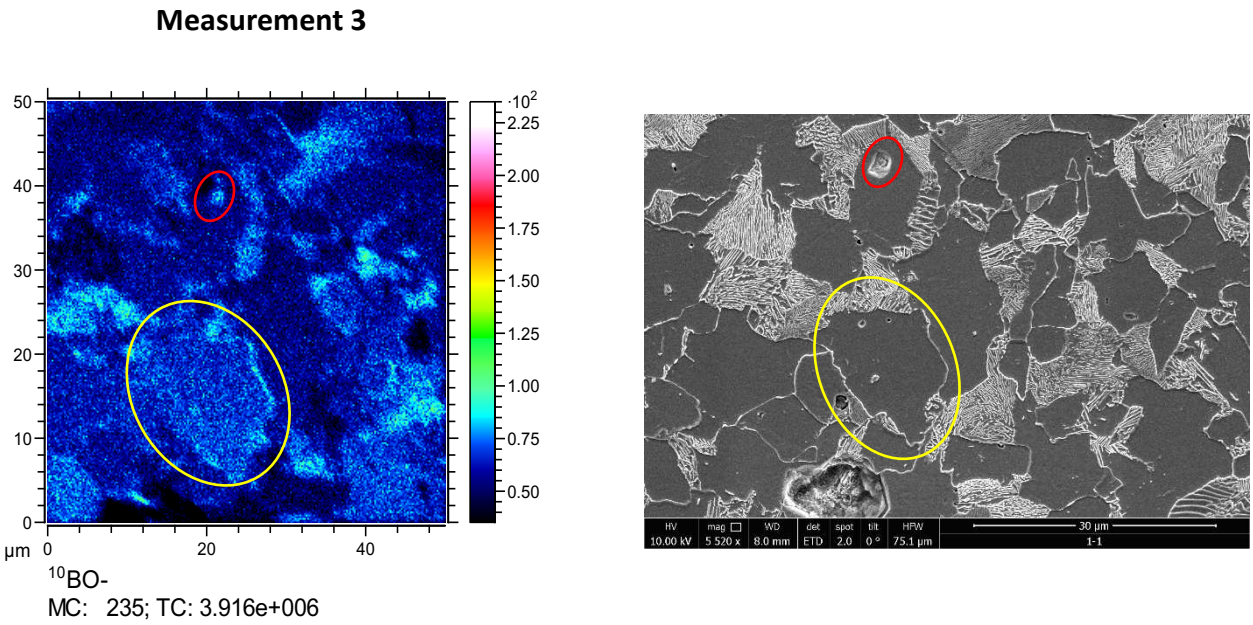

Figure 22: Assignment of elemental maps obtained by use of ToF-SIMS (left) to corresponding phases of microstructures displayed by use of FEG-SEM (right).

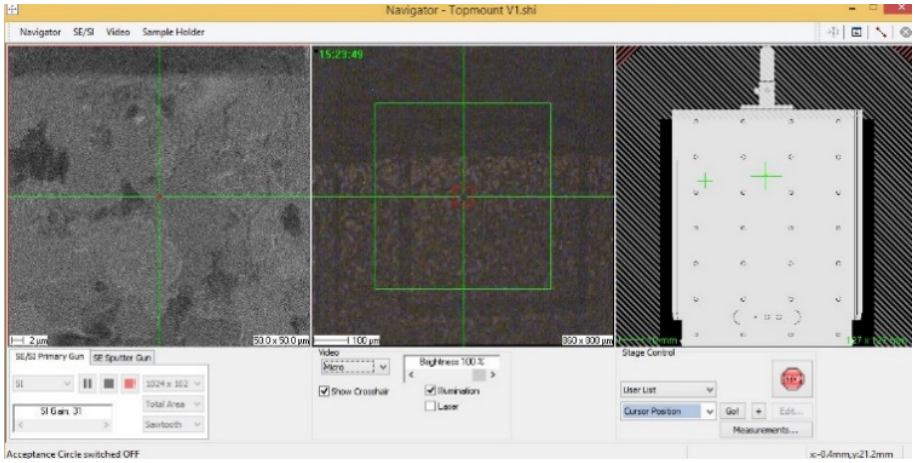

Figure 23: Screenshot of the measurements position of ToF-SIMS: The secondary ion image on the left shows the field of view including grain boundaries. In the centre, an image of the position of the field of view in relation to the pre-sputtered frame is provided. The picture in the right shows the position of the measurement in relation to the sample holder position.

Measurement 4

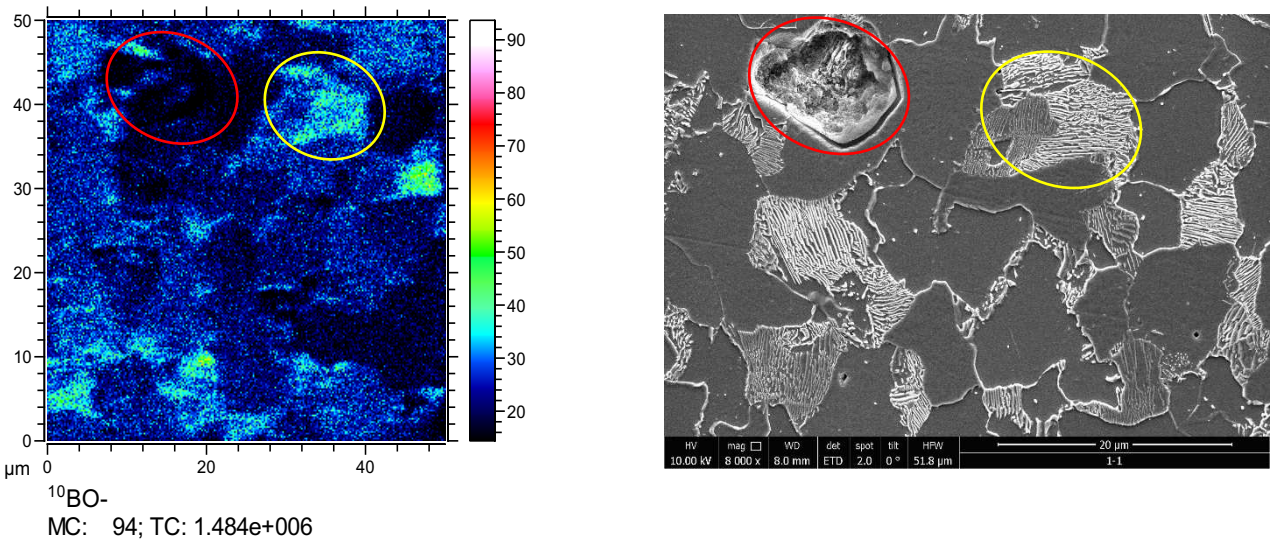

Figure 24: Assignment of elemental maps obtained by use of ToF-SIMS (left) to corresponding phases of microstructures displayed by use of FEG-SEM (right).

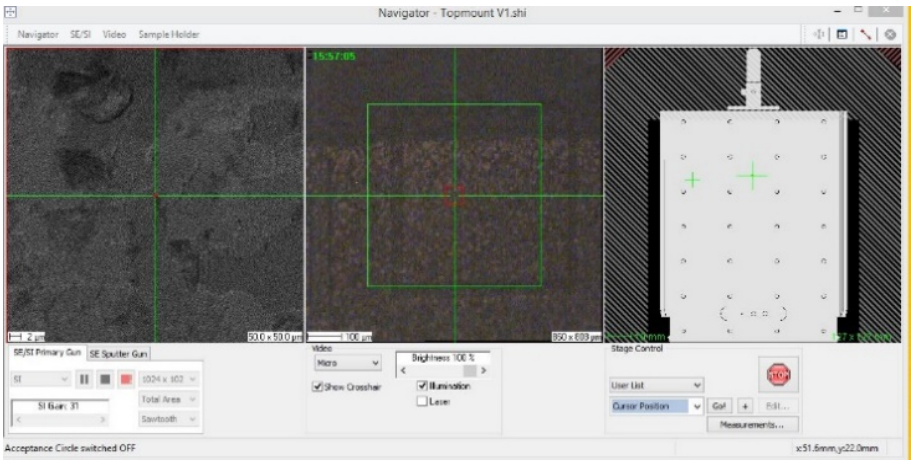

Figure 25: Screenshot of the measurements position of ToF-SIMS: The secondary ion image on the left shows the field of view including grain boundaries. In the centre, an image of the position of the field of view in relation to the pre-sputtered frame is provided. The picture in the right shows the position of the measurement in relation to the sample holder position.

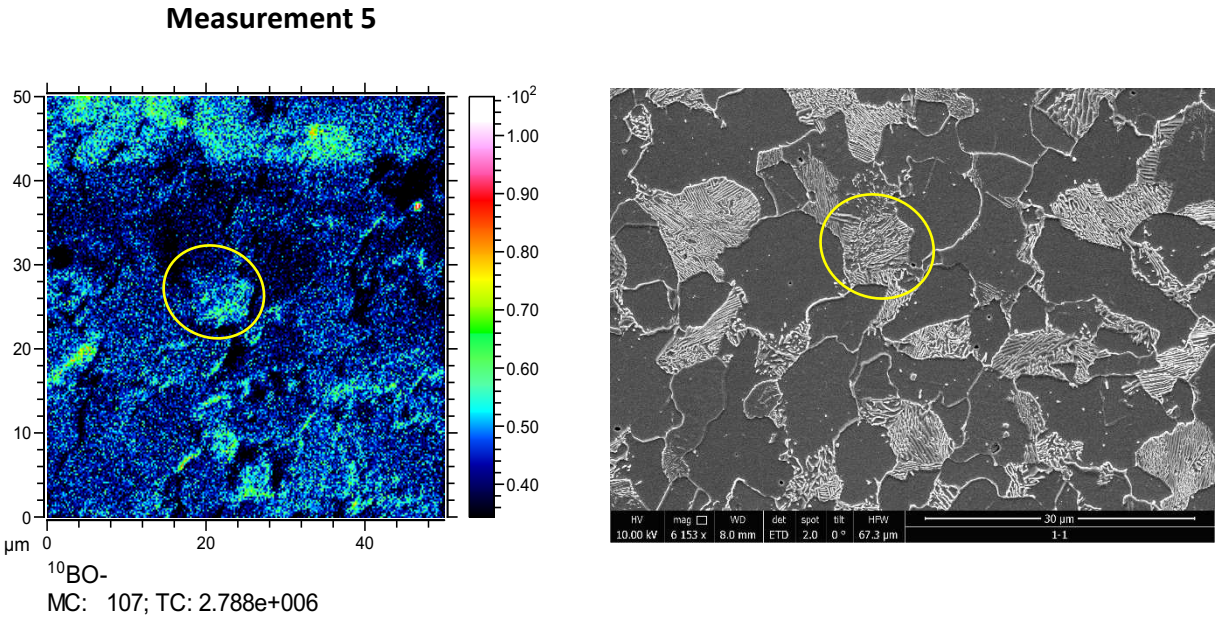

Figure 29: Assignment of elemental maps obtained by use of ToF-SIMS (left) to corresponding phases of microstructures displayed by use of FEG-SEM (right).

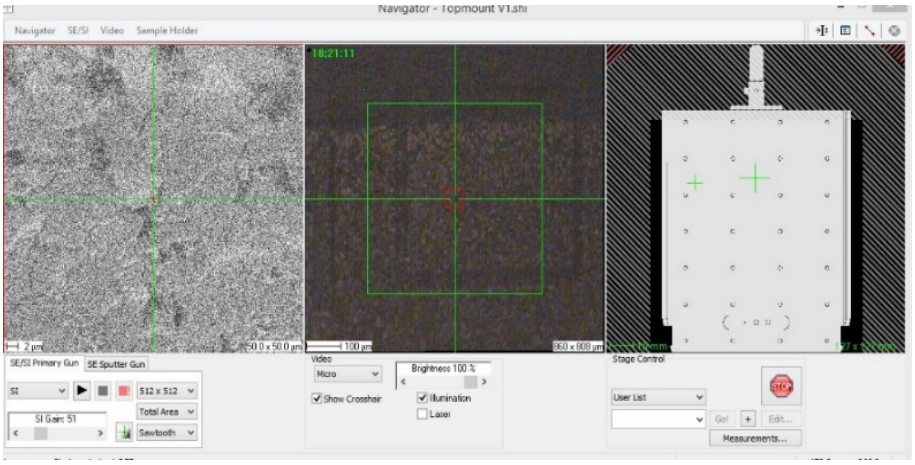

Figure 26: Screenshot of the measurements position of ToF-SIMS: The secondary ion image on the left shows the field of view including grain boundaries. In the centre, an image of the position of the field of view in relation to the pre-sputtered frame is provided. The picture in the right shows the position of the measurement in relation to the sample holder position.

Our experiments showed, that ToF-SIMS is a powerful tool for studies concerning elemental distribution of trace elements with spatial resolution in the sub 200 nm region. By utilization

of the opportunity to monitor specific isotopes it is possible to avoid wrong classifications that are caused by peak overlap when operating the device under conditions of reduced mass resolution. Therefore, it is possible to determine the distribution of B oxides in steels with a content of Al, even though the nominal masses of boron and alumina oxides are the same. Our experiments showed, that B preferential segregates within grains of pearlite whereas its concentration in ferrite grains is vanishing. By precise analysis of the boron distribution in context to the steps of forming a deeper understanding of the various transitions taking part during these steps can be achieved.

3.2) Diffusion Kinetics of isotopically pure 41K in Feldspars

For implementation of a model for age determination of feldspar containing minerals, the depth of diffusion of isotopically pure ^{41}K into bulk rock material was investigated by use of ToF-SIMS in non-interlaced mode with CBA beam guidance. As shown by Holzlechner et al. [42] isotope ratios are represented more reliable in CBA not only for oxygen tracer diffusion studies but also for diffusion of alkali metals. Any measurement was performed until the depth of constant elemental concentration of Si, Na, ^{39}K and total K was reached. Subsequently, the depths of all craters were determined by use of a Bruker DektakXT stylus profilometer. The obtained values were added to the measured depth profiles during data reconstruction. The specific intensities and corresponding values for depth were exported as ASCII files and plotted by use of OriginLab. The measurement conditions of the ToF.SIMS 5 are illustrated in table 3.

		Energy	Crater Size
LMIG	*Bi+*	*25 keV*	*50 * 50 µm*
DSC	*O2*	*2 keV*	*250 * 250 µm*
Raster Mode	*random*		
Cycle Time	*35 µs*		
Pixels	*64 * 64*		
Non-interlaced Mode	*2 frames*	*2 s sputtering*	*1 s pause*

Table 3: Standard operation conditions for ToF-SIMS measurements connected to tracer diffusion experiments on isotopically pure ^{41}K in feldspars

With the data obtained in these experiments and by knowledge of the crystal site and the conditions of the previous temperature treatment of the independent samples, the department of lithosphere research at the institute of geology (Uni Wien) is developing a method for age determination of feldspars. The depth profiles of two different specimens are shown in figures 31 and 32.

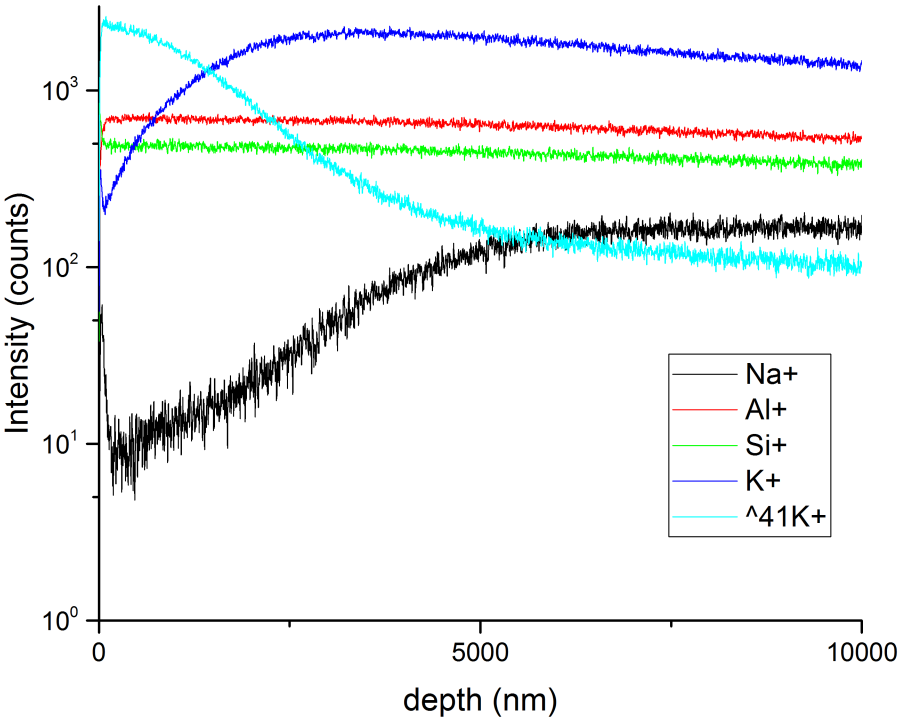

Figure 27: Tracer diffusion experiments in feldspars: The surface of the specimen was enriched with isotopically pure 41K. By determination of the depth of diffusion to corresponding crystal sites and temperature treatments of the samples it is possible to develop methods for age determination of feldspar based rock materials. In the illustrated sample, the diffusant penetrated the feldspar to a depth of about 10 µm.

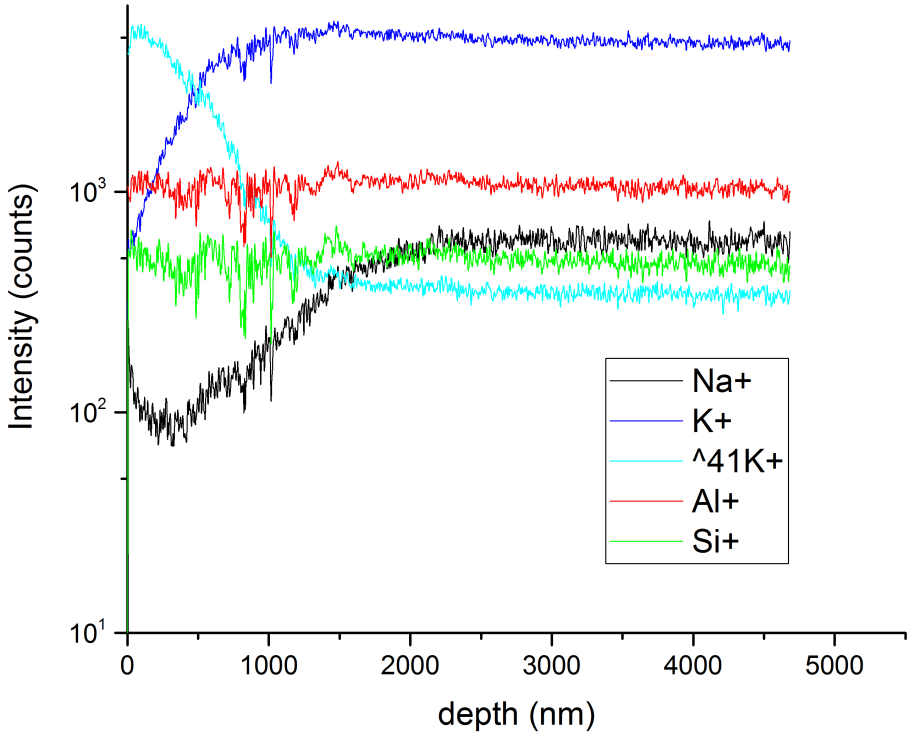

Figure 28: Tracer diffusion experiments in feldspars: The surface of the specimen was enriched with isotopically pure 41K. By determination of the depth of diffusion to corresponding crystal sites and temperature treatments of the samples, it is possible to develop methods for age determination of feldspar based rock materials. In the illustrated sample, the diffusant penetrated the feldspar to a depth of about 2 µm. The instabilities in the low depth region of the presented spectrum refer to fluctuations in the emission current of the LMIG.

By determination of the depth of diffusion of isotopically pure ^{41}K into different feldspar materials as a function of material composition, crystal site and temperature treatment, it is possible to develop a model describing the mechanisms of rock formation facilitating global age-determination of feldspar based minerals. Additionally, it was possible to show, that application of ToF-SIMS in CBA mode provides advantages as isotope ratios are expressed more reliable and the reduced intensity impedes saturation of the detector unit.

3.3) High Temperature Diffusion Kinetics of Al in Metal Layer Systems

For successful determination of diffusive properties by use of the first arrival approach, detection of the observed species has to be very sensitive. This requirement is hit by Al in the positive ion mode. Measurements were performed on a field of view of 300*300 µm with a resolution of 128*128 pixels resulting in a lateral resolution of between 10 and 20 µm. For improved understanding, evaluation of data was performed by use of the Al^+ as well as the Al^{2+} diffusion profile in order to compare the methods in terms of repeatability and accuracy.

An example for a typical diffusion profile of the observed systems is provided in figure 30. Plotting was executed by use of OriginLab. For evaluation of data, the region following the apparel of the first traces of Al on the surface was linearly fitted to determine the first arrival time for Al^+ as well as Al^{2+} for any independent measurement. The intersection point of this linear fit with the baseline, that was defined as the mean value plus two standard deviations of the region of quasi-zero Al concentration was taken to be the first arrival time. By use of formula 11 the diffusion constants for all systems were calculated. After conversion to the form of formula 5, Arrhenius plots were drawn in order to determine the activation energies for diffusion in various samples, which can be calculated by dividing the slope of the function by minus R, where R is the universal gas constant (R = 8.3145 J/K*mol). All data obtained in these experiments are plotted in the following (figures 30 to 35). The amount of nitrogen applied is given in standard cubic centimetres per minute (sccm), describing the particle stream of gas during material processing. A summary of the different investigated samples is given in table 4, the operation conditions for the measuring device are given in table 5.

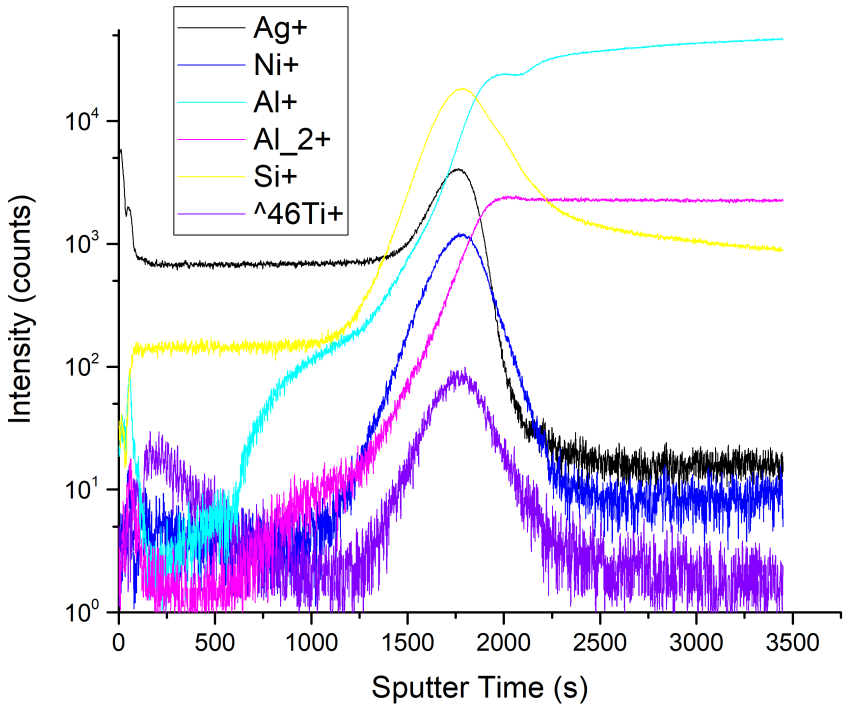

Figure 29: Typical diffusion profile of a metal layer system investigated by use of ToF-SIMS: It can be seen, that Ag is detected first and that the remaining layers are subsequently measured until a constant concentration of Al+ and Al2+ indicates the end of the diffusion experiment. By fitting linear slopes into the concentration gradient of aluminium ions, it is possible to determine the diffusion constants and consequently calculate the corresponding activation energies.

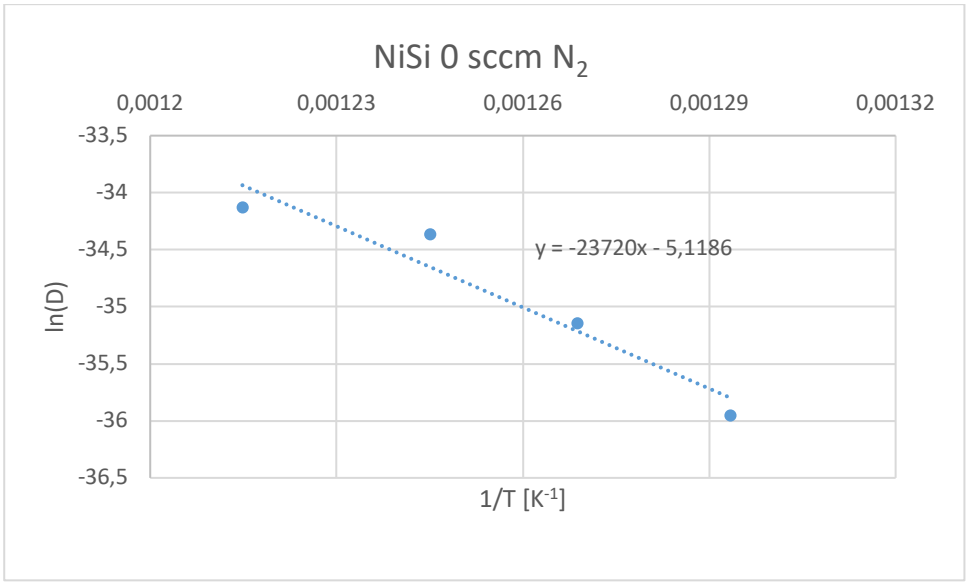

Figure 30: Arrhenius-plot of the difffusion of Al^{2+}in metal layer systems with NiSi solder that were not treated with nitrogen gas during manufacturing/processing. Determination of the activation energy is achieved by multiplication of the slope of the linear fit with the negative value of the general gas constant (R).

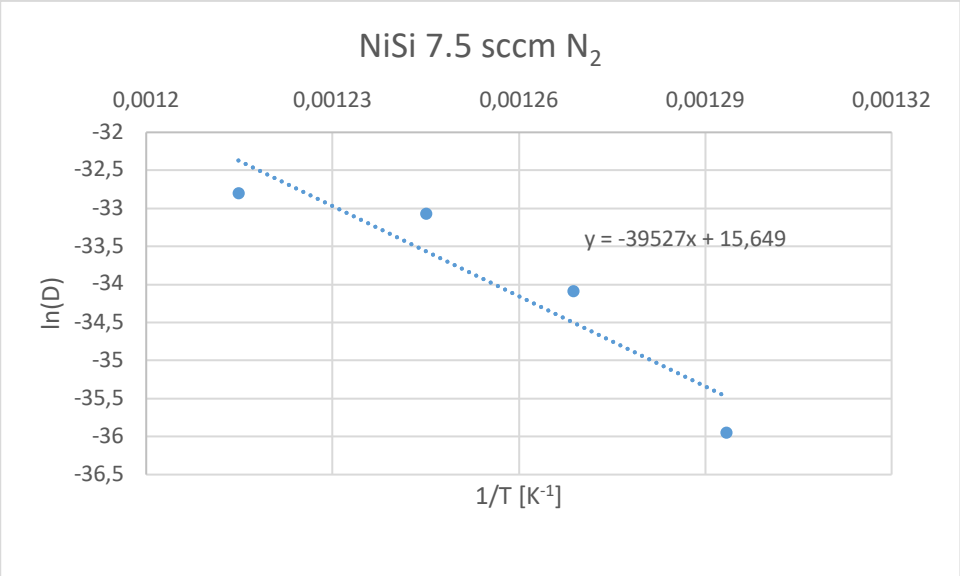

Figure 31: Arrhenius-plot of the diffusion of Al^{2+} in metal layer systems with NiSi solder that were treated with 7.5 sccm nitrogen gas during manufacturing/processing. Determination of the activation energy is achieved by multiplication of the slope of the linear fit with the negative value of the general gas constant (R).

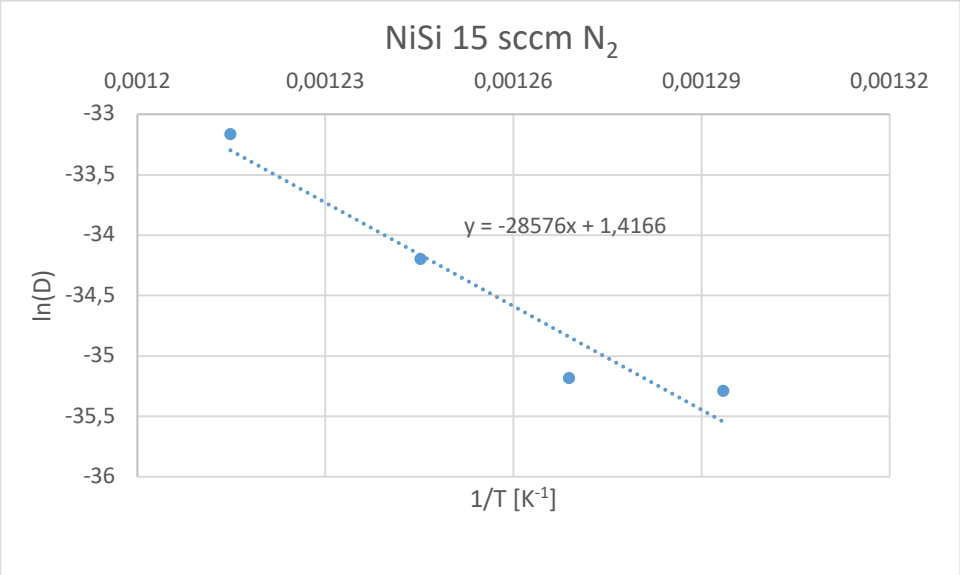

Figure 32: Arrhenius-plot of the diffusion of Al^{2+} in metal layer systems with NiSi solder that were treated with 15 sccm nitrogen gas during manufacturing/processing. Determination of the activation energy is achieved by multiplication of the slope of the linear fit with the negative value of the general gas constant (R).

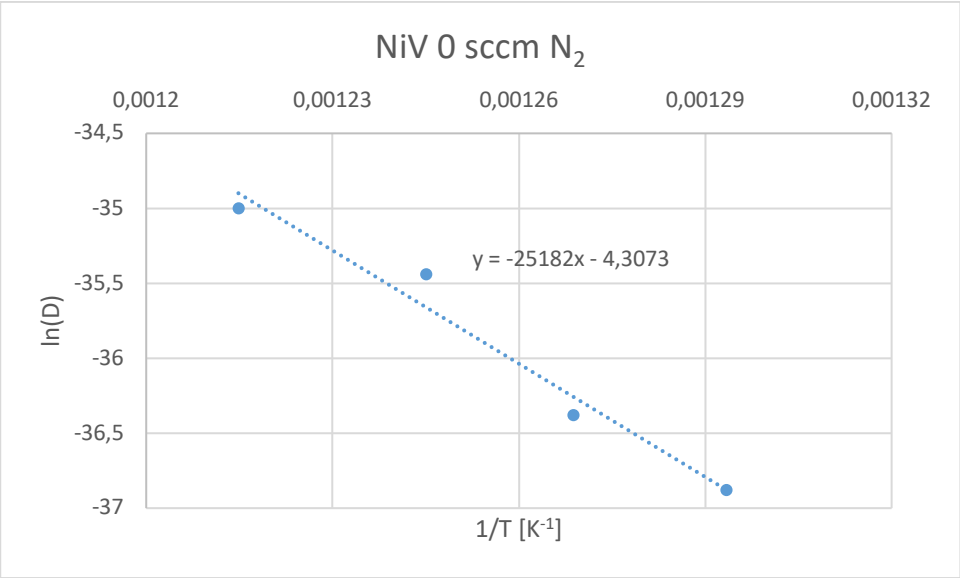

Figure 33: Arrhenius-plot of the difffusion of Al^{2+}in metal layer systems with NiV solder that were not treated with nitrogen gas during manufacturing/processing. Determination of the activation energy is achieved by multiplication of the slope of the linear fit with the negative value of the general gas constant (R).

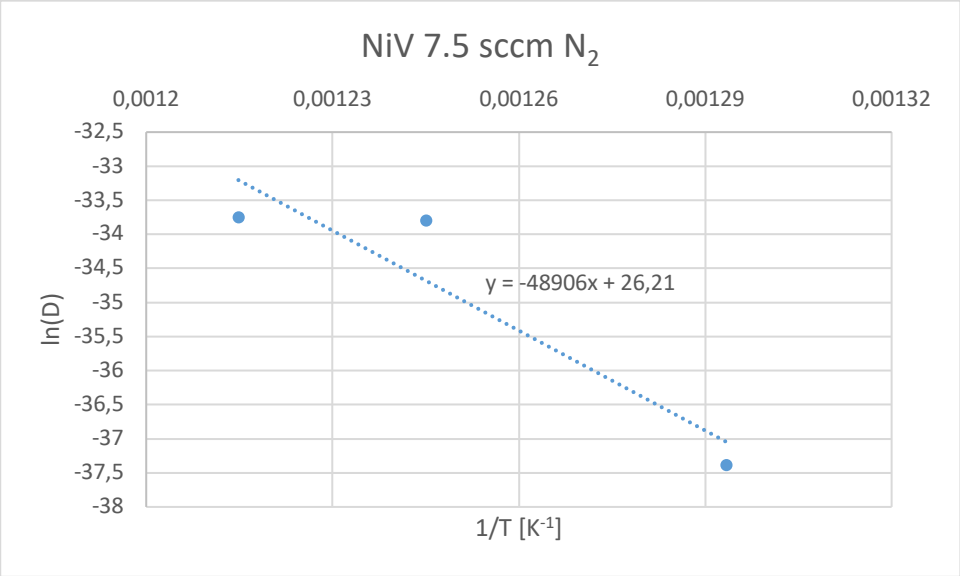

Figure 34: Arrhenius-plot of the difffusion of Al^{2+}in metal layer systems with NiV solder that were treated with 7.5 sccm nitrogen gas during manufacturing/processing. Determination of the activation energy is achieved by multiplication of the slope of the linear fit with the negative value of the general gas constant (R).

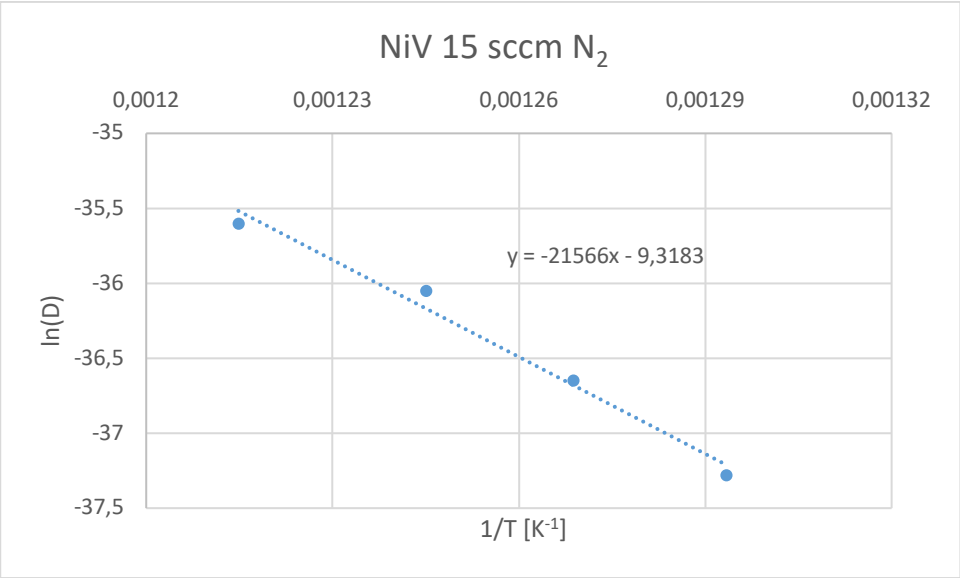

Figure 35: Arrhenius-plot of the diffffusion of Al^{2+}in metal layer systems with NiV solder that were treated with 15 sccm nitrogen gas during manufacturing/processing. Determination of the activation energy is achieved by multiplication of the slope of the linear fit with the negative value of the general gas constant (R).

Solder	N_2	E_A [kJ]	E_A [eV]
NiSi	0 sccm	197,22	2,04
NiSi	7.5 sccm	328,65	3,41
NiSi	15 sccm	237,60	2,46
NiV	1 sccm	209,38	2,17
NiV	7.5 sccm	406,63	4,21
NiV	15 sccm	179,31	1,86

Table 4: Summary of the different samples investigated and calculated activation energies for Al diffusion.

		Energy	Crater Size
LMIG	*Bi+*	*25 keV*	*300 * 300 µm*
DSC	*O2*	*2 keV*	*1000 * 1000 µm*
Raster Mode	*random*		
Cycle Time	*65 µs*		
Pixels	*128 * 128*		
Interlaced Mode			

Table 5: Standard operation conditions for ToF-SIMS measurements connected to diffusion applications in temperature programmed SIMS

Evaluation of data indicates, that the activation energy for diffusion is maximized for samples that were treated with 7.5 sccm nitrogen gas during manufacturing and processing. The results are very similar for diffusion of Al^{+} as well as Al^{2+}. For understanding of this behavior it is necessary to perform further ToF-SIMS measurements and vary the nitrogen content over a narrower region to determine the concentration of lowest diffusion probability.

Reference List:

[1] Vickermann, J. C., Briggs, D., (2001), ToF-SIMS Surface Analysis by Mass Spectrometry, IM Publications, Huddersfield (GB), p. 1-12

[2] Vickermann, J. C., Briggs, D., (2001), ToF-SIMS Surface Analysis by Mass Spectrometry, IM Publications, Huddersfield (GB), p. 95f

[3] Jaworek, A., (2007), Micro- and nanoparticle production by electrospraying, Powder Technology, vol. 176, no. 1, p. 18-35

[4] Vickermann, J. C., Briggs, D., (2001), ToF-SIMS Surface Analysis by Mass Spectrometry, IM Publications, Huddersfield (GB), p. 96

[5] Vickermann, J. C., Briggs, D., (2001), ToF-SIMS Surface Analysis by Mass Spectrometry, IM Publications, Huddersfield (GB), p. 96

[6] Vickermann, J. C., Briggs, D., (2001), ToF-SIMS Surface Analysis by Mass Spectrometry, IM Publications, Huddersfield (GB), p. 3

[7] Sigmund, P., (1984), Fundamentals of Sputtering - Secondary Ion Mass Spectrometry SIMS IV, Springer, Odense (DEN), p. 2-7

[8] Kenneth, L., et al., (1983), Matrix effects in secondary ion mass spectrometry, Anal. Chem., vol. 55, no. 7, p. 1157-1160

[9] Reed, N. M., et al., in: Vickermann, J. C., Briggs, D., (2001), ToF-SIMS Surface Analysis by Mass Spectrometry, IM Publications, Huddersfield (GB), p. 9

[10] Website IONTOF GmbH, (2018), https://www.iontof.com/charge-compensation-tof-sims-5.html, 18.03.2019, IONTOF, Münster

[11] Vickermann, J. C., Briggs, D., (2001), ToF-SIMS Surface Analysis by Mass Spectrometry, IM Publications, Huddersfield (GB), p. 75

[12] Vickermann, J. C., Briggs, D., (2001), ToF-SIMS Surface Analysis by Mass Spectrometry, IM Publications, Huddersfield (GB), p. 75-93

[13] Amoruso, S., et al., (1999), Characterization of Laser-Ablation Plasmas, J. of Physics B Atomic Molecular and Optical Physics, vol. 33, no. 14, Naples (I)

[14] Vickermann, J. C., Briggs, D., (2001), ToF-SIMS Surface Analysis by Mass Spectrometry, IM Publications, Huddersfield (GB), p. 7

[15] Vickermann, J. C., Briggs, D., (2001), ToF-SIMS Surface Analysis by Mass Spectrometry, IM Publications, Huddersfield (GB), p. 102ff

[16] Holzlechner, G., et al., (2013) A novel ToF-SIMS operation mode for improved accuracy and lateral resolution of oxygen isotope measurements on oxides, J. Anal. At. Spectrom, vol. 28, p. 1080-1089

[17] Kubicek, M., et al., (2014) A novel ToF-SIMS operation mode for sub 100 nm lateral resolution: Application and performance, Applied Surface Science, vol. 289, p. 408

[18] Vickermann, J. C., Briggs, D., (2001), ToF-SIMS Surface Analysis by Mass Spectrometry, IM Publications, Huddersfield (GB), p. 100

[19] Rose, H. H., (2008), Optics of high-performance electron microscopes, Sci. Technol. Adv. Mater., vol. 9, no. 1

[20] Jede R., Peters, H., (1986), Analyse dünner Schichten mittels Massenspektrometrie zerstäubter Neutralteilchen, Technisches Messen, vol. 11, p. 407-413

[21] Schnöller, J., (2009), ToF-SIMS – A Versatile Technique in Analytical Chemistry, Dissertation, Vienna, p. 29f

[22] Wikipedia: The Free Encyclopedia, (2019), Stigmator, https://en.wikipedia.org/wiki/Stigmator, 18.03.2019

[23] Website IONTOF GmbH, (2018), https://www.iontof.com/download/IONTOF_TOF-SIMS-5_Patented-Burst-Mode.pdf, 18.03.2019, IONTOF, Münster

[24] Kubicek, M., et al., (2014) A novel ToF-SIMS operation mode for sub 100 nm lateral resolution: Application and performance, Applied Surface Science, vol. 289, p. 408

[25] Amsüss, A., Diffusion and Phase Formation in the Al-Cu Thin Film System…, Dissertation, (2019), TU Vienna, Vienna (AUT), p. 3f

[26] Crank, J., The Mathematics of Diffusion, 2nd edition, (1979), Oxford University Press, Maidenhead (GB), p. 1

[27] Amsüss, A., Diffusion and Phase Formation in the Al-Cu Thin Film System…, Dissertation, (2019), TU Vienna, Vienna (AUT), p. 4-6

[28] Gupta, D., Ho, P. S., Diffusion Processes in Thin Films, (1980), Thin Film Solids, vol. 72, p. 399-418

[29] Moritani, K. et al., Extremely low-energy projectiles for SIMS using size-selected gas cluster ions, (2008), Appl. Surf. Sci., vol. 255, p. 948-950

[30] Matsuo, J. et al., What size of cluster is most appropriate for SIMS?, (2008), Appl. Surf. Sci., vol. 255, p. 1235-1238

[31] Amsüss, A., Diffusion and Phase Formation in the Al-Cu Thin Film System…, Dissertation, (2019), TU Vienna, Vienna (AUT)

[32] Tanaka, H., Hayashi, S., Analysis of the Distribution of Light Elements in Steels by ToF-SIMS, (2018), Nippon Steel and Sumitomo Metal Technical Report, no. 118, p. 27-33

[33] Song, T., De Cooman, B., (2012), Effect of Boron on the Isothermal Bainite Transformation, Metallurgiacal and Materials Transactions A, vol. 44

[34] University of Tennessee, Dept. Of Materials Science and Engineering, Iron-Carbon Phase Diagram (a review), https://web.utk.edu/~prack/MSE%20300/FeC.pdf

[35] Wikiwand, (2018), Feldspar, http://www.wikiwand.com/en/Feldspar, 22.03.2019, San Francisco (USA)

[36] Wikiwand, (2018), Feldspar, http://www.wikiwand.com/en/Feldspar, 22.03.2019, San Francisco (USA)

[37] Heuser, D., (2016), Kalium Selbstdiffusion in Feldspäten, Master Thesis, http://othes.univie.ac. at/44546/1/46586.pdf, Institute for Geology (Uni Vienna), p. 3-7

[38] E Apodaca, L., (2008), Feldspar and Nepheline Syenite, 2008 Minerals Yearbook, U.S. Deparment of the Interior, https://minerals.usgs.gov/minerals/pubs/commodity/feldspar/myb1-2008-felds.pdf, 22.03.2019

[39] Heuser, D., (2016), Kalium Selbstdiffusion in Feldspäten, Master Thesis, http://othes.univie.ac. at/44546/1/46586.pdf, Institute for Geology (Uni Vienna), p. 21-29

[40] Holzlechener, G., et al., (2013), A Novel ToF-SIMS Operation Mode for Improved Accuracy and Lateral Resolution of Oxygen Isotope Measurements on Oxides, Journal of Analytical Atomic Spectrosopy, vol. 28, p. 1080-1090

[41] Bruker, (2011), Brochure for Dektak XT Stylus Profiler, https://www.bruker.com/fileadmin/user_upload/8-PDF-Docs/SurfaceAnalysis/StylusProfilometry/Brochures/B516-RevB2-DektakXT_Stylus_Profiler-Brochure.pdf , Bruker Nano Surfaces Division, Tucson (USA), 22.03.2019

[42] Holzlechener, G., et al., (2013), A Novel ToF-SIMS Operation Mode for Improved Accuracy and Lateral Resolution of Oxygen Isotope Measurements on Oxides, Journal of Analytical Atomic Spectrosopy, vol. 28, p. 1080-1090